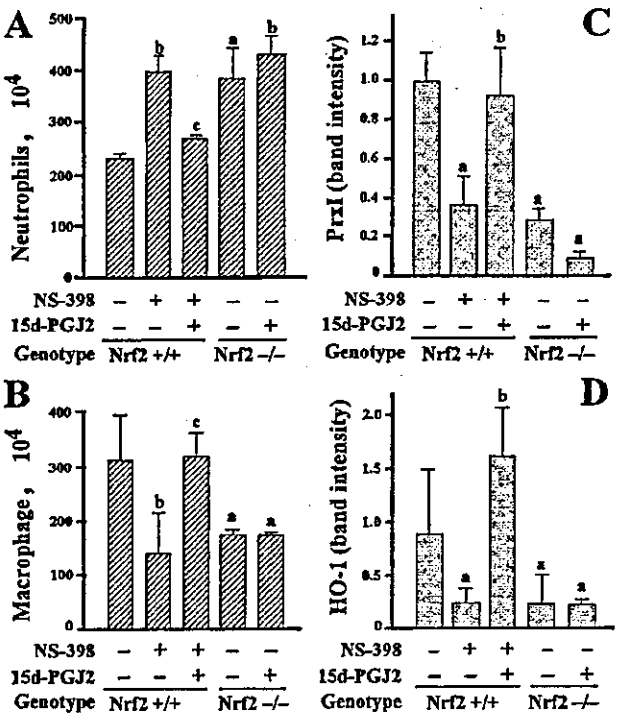

FIG. 6. Intrapleural injection of 15d-PGJ_2 reverses the decrease of PrxI expression and persistence of neutrophils in NS-398-treated mice but not in Nrf2-deficient mice. (A and B) Numbers of neutrophils (A) and macrophages (B) at 24 h of pleurisy in wild-type ($nrf2^{+/+}$) mice (bars 1), NS-398-treated $nrf2^{+/+}$ mice (bars 2), NS-398-treated $nrf2^{+/+}$ mice administrated 15d-PGJ_2 (bars 3), $nrf2^{-/-}$ mice (bars 4), and $nrf2^{-/-}$ mice administrated NS-398 (bars 5). Neutrophils and macrophages were counted microscopically, and the means and standard deviations of triplicates are shown. a, $P < 0.05$ compared with untreated control mice; b, $P < 0.01$ compared with untreated control mice; c, $P < 0.01$ compared with NS-398-treated wild-type mice. (C, D) RT-PCR analysis of PrxI (C) and HO-1 (D) mRNAs in pleural inflammatory cells in mice. Intensities of RT-PCR bands were quantified by densitometric analysis, and the means of triplicates are presented. a, $P < 0.01$ compared with untreated control group; b, $P < 0.01$ compared with NS-398-treated wild-type mice.

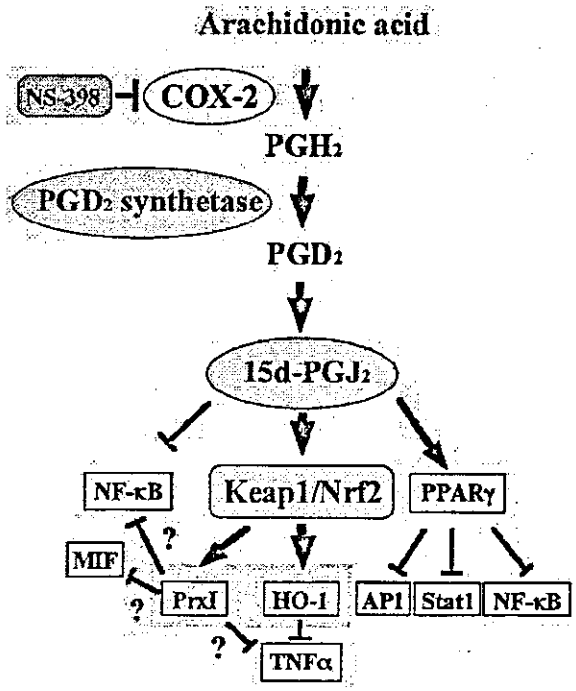

FIG. 7. Network of 15d-PGJ_2 and the Nrf2-Keap1 pathway in carrageenan-induced pleurisy. 15d-PGJ_2 is generated in pleural macrophages during carrageenan-induced pleurisy and is known to directly inhibit NF-κB activity and also to act as a ligand for PPARγ. This study shows that 15d-PGJ_2 activates the Nrf2-Keap1 pathway through covalent binding to Keap1. Nrf2 induces HO-1 and PrxI expression as well as other ARE-regulated genes in macrophages (green). The upregulation of PrxI appears to inhibit NF-κB, TNF-α, and the β-tautomerase activity of MIF, thus modulating the inflammation process. On the other hand, HO-1 is known to inhibit the expression of TNF-α through CO production.

that 15d-PGJ_2 inhibits NF-κB activation by covalently binding to IκB kinase β or the p50 subunit of NF-κB (3, 36). In addition, 15d-PGJ_2 has been reported to serve as a natural ligand of PPARγ (21, 34). Activated PPARγ regulates the synthesis of proinflammatory cytokines and the induction of nitric oxide synthetase in activated monocytes by negatively interacting with AP-1, NF-κB, or STAT. Thus, 15d-PGJ_2 may have an impact upon multiple mechanisms during the resolution of inflammation. The results of this study demonstrate that 15d-PGJ_2 can act as a potent anti-inflammatory agent by exploiting the Nrf2-Keap1 pathway, a previously unrecognized alternative pathway in the cascades downstream of 15d-PGJ_2.

The possible involvement of Nrf2 in inflammation has been alluded to in some earlier reports. For instance, antirheumatic gold(I) compounds markedly activate Nrf2 (24). We found that female Nrf2 knockout mice frequently developed severe glomerulonephritis (46). Braun et al. recently reported that Nrf2 regulates inflammation during healing of skin wounds (2). The expression of several inflammatory cytokines was shown to persist during the healing of a skin wound in Nrf2-deficient mice, such that interleukin-1β levels in the wound remained elevated to day 13, most likely due to the persistence of macrophages at the site of the wound. Finally, ARE battery genes are activated by laminar shear stress, which acts as an anti-inflammatory signal in endothelial cells (6). Indeed, in endothelial cells, overexpression of Nrf2 inhibited the tumor necrosis factor alpha (TNF-α)-mediated induction of vascular cell adhesion molecule-1 gene expression, which is important for monocyte recruitment during inflammation response. Our present observations, along with those cited above, suggest that Nrf2 is important for regulating the process of acute inflammation.

We demonstrated in this study that the intracellular accumulation of 15d-PGJ_2 occurs during carrageenan-induced pleurisy in the mouse (Fig. 2). This observation is consistent with the previous analysis in rat carrageenan pleurisy, where 15d-PGJ_2 accumulates with two peaks at low nanomolar levels in the pleural exudates. As the 15d-PGJ_2 concentration used in this study is higher than that detected in pleural exudates, it might be challenging to hypothesize that 15d-PGJ_2 works as an endogenous regulator of acute inflammation. However, Narumiya et al. previously reported that exogenously added Δ^{12}-

PGJ_2 accumulates in the cells in a protein-bound form and is resistant to cell extraction, suggesting that intracellular sequestration of these cyPGs is most probably due to the Michael adduction to the protein (27). Furthermore, Keap1 localizes in the perinuclear cytoskeleton close to COX-2 and PGDS. Therefore, it is likely that the local concentration of cyPGs accumulates to a level sufficient for Nrf2 activation during pleurisy.

It was reported recently that submicromolar concentrations of 15d-PGJ_2 can activate HO-1 and contribute to the anti-inflammatory effect of this reagent (25). As NF-κB inhibition requires a concentration of 15d-PGJ_2 in the micromolar range in cell culture (36), this observation suggests that an in vivo anti-inflammatory effect of 15d-PGJ_2 may be more relevant to the activation of Nrf2.

Under normal conditions, Nrf2 activity is suppressed primarily by its compartmentalization to the cytosol by Keap1 and consequent rapid degradation by the proteasome (reference 20 and references therein). Recently it was demonstrated that electrophiles classified as Michael reaction acceptors directly bound to Keap1 and dissociated Nrf2 from Keap1 (9). We have demonstrated in this study that 15d-PGJ_2 and Δ^{12}-PGJ_2, both of which contain a reactive α,β-unsaturated carbonyl group in their cyclopentane ring, directly bind to Keap1 and activate Nrf2. These results are consistent with our contention that cyPGs act as endogenous activators of the Nrf2-Keap1 pathway in macrophages, thereby regulating the recruitment of inflammatory cells.

NS-398-treated wild-type mice and *nrf2*-null mice displayed similar phenotypes in pleurisy, i.e., a persistence of neutrophil residence and a delay in macrophage recruitment. These results suggest that COX-2 products negatively regulate the accumulation of neutrophils in the intrapleural space, through either enhancing the phagocytosis of neutrophils by macrophages or decreasing the neutrophil infiltration. The administration of 15d-PGJ_2 into the pleural space successfully reversed the phenotype in NS-398-treated mice, indicating that 15d-PGJ_2 works downstream of COX-2 activation. Consistent with this observation, we demonstrated in this study that the actual inducible accumulation of 15d-PGJ_2 occurred in macrophages during carrageenan pleurisy (Fig. 2). Since the introduction of 15d-PGJ_2 into the pleural spaces of Nrf2-deficient mice had no effect, Nrf2 must be a downstream mediator of 15d-PGJ_2 activity in macrophages. Thus, we conclude that 15d-PGJ_2 regulates acute inflammation through regulating the function of macrophages (Fig. 7).

It remains to be elucidated to how Nrf2 regulates acute inflammation. We speculate that a battery of Nrf2 target genes cooperatively function to repress proinflammatory signals, such as those of TNF-α or interleukin-1β. HO-1 and PrxI are the Nrf2 target genes that are likely to influence the inflammatory process (Fig. 7) (16). Recently, Gong et al. have demonstrated that 15d-PGJ_2 can activate HO-1 via a stress-responsive element and by an Nrf2-mediated mechanism (14). In the carrageenan-induced pleurisy model, it has been shown that elevation of HO-1 expression can suppress, whereas inhibition of HO-1 activity can exacerbate, the inflammatory response (43, 45). Indeed, HO-1 can inhibit the expression of TNF-α most probably through the generation of carbon monoxide (30). With respect to PrxI, its human counterpart PAG was reported to directly bind to and negatively regulate β-tautomerase activity of MIF, which is one of the central regulators of inflammation (22). Although the physiological significance of the β-tautomerase activity of MIF is unclear at present, we nonetheless expect that the repression of MIF activity by PrxI may play important roles in the regulation of inflammation. Furthermore, the overexpression of PrxI removed H_2O_2 (23), suggesting that PrxI can repress TNF-α signaling by the removal of H_2O_2 (Fig. 7). These observations suggest that Nrf2 may have multiple downstream targets that regulate the acute inflammation process.

In the rat carrageenan-induced pleurisy model, accumulation of 15d-PGJ_2 in the late phase of pleurisy was associated with resolution of the inflammation (13). However, the true role of 15d-PGJ_2 during the early phase of pleurisy remained largely unknown. Our results imply that in the early phase, accumulation of 15d-PGJ_2 activates Nrf2 and regulates the inflammation process through the induction of target gene expression, including that of HO-1 and PrxI. Whereas COX-2 has been reported to accelerate inflammation in the early phase of pleurisy through the induction of PGE_2, our present analyses suggest that COX-2 also can suppress the early phase of inflammation through the production of 15d-PGJ_2. These results are consistent with the present model that the inflammation process is balanced by an acceleration and deceleration of integrating signaling pathways (28). Understanding of how the signals are integrated to establish and resolve the acute inflammation process provides important clues to facilitate the development of effective treatments for chronic inflammation.

ACKNOWLEDGMENTS

We thank S. Taketani for providing the polyclonal antibody against rat HO-1. We also thank Y. Katoh, A. Kobayashi, M. Kobayashi, S. Nishimura, K. I. Tong, and N. Wakabayashi for discussion and advice.

This work was supported in part by grants from JST-ERATO; the Ministry of Education, Culture, Sports, Science and Technology; the Ministry of Health, Labor and Welfare; and the Naito foundation.

REFERENCES

1. **Aoki, Y., H. Sato, N. Nishimura, S. Takahashi, K. Itoh, and M. Yamamoto.** 2001. Accelerated DNA adduct formation in the lung of the Nrf2 knockout mouse exposed to diesel exhaust. Toxicol. Appl. Pharmacol. 173:154–160.
2. **Braun, S., C. Hanselmann, M. G. Gassmann, U. auf dem Keller, C. Born-Berclaz, K. Chan, Y. W. Kan, and S. Werner.** 2002. Nrf2 transcription factor, a novel target of keratinocyte growth factor action which regulates gene expression and inflammation in the healing skin wound. Mol. Cell. Biol. 22:5492–5505.
3. **Cernuda-Morollon, E., E. Pineda-Molina, F. J. Canada, and D. Perez-Sala.** 2001. 15-Deoxy-$\Delta^{12,14}$-prostaglandin J_2 inhibition of NF-κB-DNA binding through covalent modification of the p50 subunit. J. Biol. Chem. 276:35530–35536.
4. **Chan, K., and Y. W. Kan.** 1999. Nrf2 is essential for protection against acute pulmonary injury in mice. Proc. Natl. Acad. Sci. USA 96:12731–12736.
5. **Chan, K., R. Lu, J. C. Chang, and Y. W. Kan.** 1996. NRF2, a member of the NFE2 family of transcription factors, is not essential for murine erythropoiesis, growth, and development. Proc. Natl. Acad. Sci. USA 93:13943–13948.
6. **Chen, X. L., S. E. Varner, A. S. Rao, J. Y. Grey, S. Thomas, C. K. Cook, M. A. Wasserman, R. M. Medford, A. K. Jaiswal, and C. Kunsch.** 2003. Laminar flow induction of antioxidant response element-mediated genes in endothelial cells. A novel anti-inflammatory mechanism. J. Biol. Chem. 278:703–711.
7. **Cho, H. Y., A. E. Jedlicka, S. P. Reddy, T. W. Kensler, M. Yamamoto, L. Y. Zhang, and S. R. Kleeberger.** 2002. Role of NRF2 in protection against hyperoxic lung injury in mice. Am. J. Respir. Cell. Mol. Biol. 26:175–182.
8. **Cuzzocrea, S., N. S. Wayman, E. Mazzon, L. Dugo, R. Di Paola, L. Serraino, D. Britti, P. K. Chatterjee, A. P. Caputi, and C. Thiemermann.** 2002. The cyclopentenone prostaglandin 15-deoxy-$\Delta^{12,14}$-prostaglandin J_2 attenuates the development of acute and chronic inflammation. Mol. Pharmacol. 61: 997–1007.
9. **Dinkova-Kostova, A. T., W. D. Holtzclaw, R. N. Cole, K. Itoh, N. Wakaba-**

yashi, Y. Katoh, M. Yamamoto, and P. Talalay. 2002. Direct evidence that sulfhydryl groups of Keap1 are the sensors regulating induction of phase 2 enzymes that protect against carcinogens and oxidants. Proc. Natl. Acad. Sci. USA 99:11908–11913.
10. Di Rosa, M., J. P. Giroud, and D. A. Willoughby. 1971. Studies on the mediators of the acute inflammatory response induced in rats in different sites by carrageenan and turpentine. J. Pathol. 104:15–29.
11. Enomoto, A., K. Itoh, E. Nagayoshi, J. Haruta, T. Kimura, T. O'Connor, T. Harada, and M. Yamamoto. 2001. High sensitivity of Nrf2 knockout mice to acetaminophen hepatotoxicity associated with decreased expression of ARE-regulated drug metabolizing enzymes and antioxidant genes. Toxicol. Sci. 59:169–177.
12. Fukushima, M. 1992. Biological activities and mechanisms of action of PGJ2 and related compounds: an update. Prostaglandins Leukot. Essential Fatty Acids 47:1–12.
13. Gilroy, D. W., P. R. Colville-Nash, D. Willis, J. Chivers, M. J. Paul-Clark, and D. A. Willoughby. 1999. Inducible cyclooxygenase may have anti-inflammatory properties. Nat. Med. 5:698–701.
14. Gong, P., D. Stewart, B. Hu, N. Li, J. Cook, A. Nel, and J. Alam. 2002. Activation of the mouse heme oxygenase-1 gene by 15-deoxy-$\Delta^{12,14}$-prostaglandin J_2 is mediated by the stress response elements and transcription factor Nrf2. Antioxid. Redox Signal. 4:249–257.
15. Ishii, T., K. Itoh, and M. Yamamoto. 2002. Roles of Nrf2 in activation of antioxidant enzyme genes via antioxidant responsive elements. Methods Enzymol. 348:182–190.
16. Ishii, T., K. Itoh, S. Takahashi, H. Sato, T. Yanagawa, Y. Katoh, S. Bannai, and M. Yamamoto. 2000. Transcription factor Nrf2 coordinately regulates a group of oxidative stress-inducible genes in macrophages. J. Biol. Chem. 275:16023–16029.
17. Ishii, T., M. Yamada, H. Sato, M. Matsue, S. Taketani, K. Nakayama, Y. Sugita, and S. Bannai. 1993. Cloning and characterization of a 23-kDa stress-induced mouse peritoneal macrophage protein. J. Biol. Chem. 268: 18633–18636.
18. Itoh, K., T. Chiba, S. Takahashi, T. Ishii, K. Igarashi, Y. Katoh, T. Oyake, N. Hayashi, K. Satoh, I. Hatayama, M. Yamamoto, and Y. Nabeshima. 1997. An Nrf2/small Maf heterodimer mediates the induction of phase II detoxifying enzyme genes through antioxidant response elements. Biochem. Biophys. Res. Commun. 236:313–322.
19. Itoh, K., N. Wakabayashi, Y. Katoh, T. Ishii, K. Igarashi, J. D. Engel, and M. Yamamoto. 1999. Keap1 represses nuclear activation of antioxidant responsive elements by Nrf2 through binding to the amino-terminal Neh2 domain. Genes Dev. 13:76–86.
20. Itoh, K., N. Wakabayashi, Y. Katoh, T. Ishii, T. O'Connor, and M. Yamamoto. 2003. Keap1 regulates both cytoplasmic-nuclear shuttling and degradation of Nrf2 in response to electrophiles. Genes Cells 8:379–381.
21. Jiang, C., A. T. Ting, and B. Seed. 1998. PPAR-γ agonists inhibit production of monocyte inflammatory cytokines. Nature 391:82–86.
22. Jung, H., T. Kim, H. Z. Chae, K. T. Kim, and H. Ha. 2001. Regulation of macrophage migration inhibitory factor and thiol-specific antioxidant protein PAG by direct interaction. J. Biol. Chem. 276:15504–15510.
23. Kang, S. W., H. Z. Chae, M. S. Seo, K. Kim, I. C. Baines, and S. G. Rhee. 1998. Mammalian peroxiredoxin isoforms can reduce hydrogen peroxide generated in response to growth factors and tumor necrosis factor-α. J. Biol. Chem. 273:6297–6302.
24. Kataoka, K., H. Handa, and M. Nishizawa. 2001. Induction of cellular anti-oxidative stress genes through heterodimeric transcription factor Nrf2/small Maf by antirheumatic gold(I) compounds. J. Biol. Chem. 276:34074–34081.
25. Lee, T. S., H. L. Tsai, and L. Y. Chau. 2003. Induction of heme oxygenase-1 expression in murine macrophages is essential for the anti-inflammatory effect of low dose 15-deoxy-$\Delta^{12,14}$-prostaglandin J_2. J. Biol. Chem. 278: 19325–19330.
26. Metz, C. N., and R. Bucala. 1997. Role of macrophage migration inhibitory factor in the regulation of the immune response. Adv. Immunol. 66:197–223.
27. Narumiya, S., K. Ohno, M. Fukushima, and M. Fujiwara. 1987. Site and mechanism of growth inhibition by prostaglandins. III. Distribution and binding of prostaglandin A_2 and Δ^{12}-prostaglandin J_2 in nuclei. J. Pharmacol. Exp. Ther. 242:306–311.
28. Nathan, C. 2002. Points of control in inflammation. Nature 420:846–852.
29. Negishi, M., T. Koizumi, and A. Ichikawa. 1995. Biological actions of delta 12-prostaglandin J2. J. Lipid Mediat. Cell Signal. 12:443–448.
30. Otterbein, L. E., F. H. Bach, J. Alam, M. Soares, H. Tao Lu, M. Wysk, R. J. Davis, R. A. Flavell, and A. M. Choi. 2000. Carbon monoxide has anti-inflammatory effects involving the mitogen-activated protein kinase pathway. Nat. Med. 6:422–428.
31. Prestera, T., Y. Zhang, S. R. Spencer, C. A. Wilczak, and P. Talalay. 1993. The electrophile counterattack response: protection against neoplasia and toxicity. Adv. Enzyme Regul. 33:281–296.
32. Primiano, T., T. R. Sutter, and T. W. Kensler. 1997. Antioxidant-inducible genes. Adv. Pharmacol. 38:293–328.
33. Ramos-Gomez, M., M. K. Kwak, P. M. Dolan, K. Itoh, M. Yamamoto, P. Talalay, and T. W. Kensler. 2001. Sensitivity to carcinogenesis is increased and chemoprotective efficacy of enzyme inducers is lost in nrf2 transcription factor-deficient mice. Proc. Natl. Acad. Sci. USA 98:3410–3415.
34. Ricote, M., A. C. Li, T. M. Willson, C. J. Kelly, and C. K. Glass. 1998. The peroxisome proliferator-activated receptor-γ is a negative regulator of macrophage activation. Nature 391:79–82.
35. Roger, T., J. David, M. P. Glauser, and T. Calandra. 2001. MIF regulates innate immune responses through modulation of Toll-like receptor 4. Nature 414:920–924.
36. Rossi, A., P. Kapahi, G. Natoli, T. Takahashi, Y. Chen, M. Karin, and M. G. Santoro. 2000. Anti-inflammatory cyclopentenone prostaglandins are direct inhibitors of IκB kinase. Nature 403:103–108.
37. Seibert, K., Y. Zhang, K. Leahy, S. Hauser, J. Masferrer, W. Perkins, L. Lee, and P. Isakson. 1994. Pharmacological and biochemical demonstration of the role of cyclooxygenase 2 in inflammation and pain. Proc. Natl. Acad. Sci. USA 91:12013–12017.
38. Shibata, T., M. Kondo, T. Osawa, N. Shibata, M. Kobayashi, and K. Uchida. 2002. 15-Deoxy-$\Delta^{12,14}$-prostaglandin J_2: a prostaglandin D_2 metabolite generated during inflammatory processes. J. Biol. Chem. 277:10459–10466.
39. Talalay, P., M. J. De Long, and H. J. Prochaska. 1988. Identification of a common chemical signal regulating the induction of enzymes that protect against chemical carcinogenesis. Proc. Natl. Acad. Sci. USA 85:8261–8265.
40. Vane, J. R. 1971. Inhibition of prostaglandin synthesis as a mechanism of action for aspirin-like drugs. Nat. New Biol. 231:232–235.
41. Venugopal, R., and A. K. Jaiswal. 1996. Nrf1 and Nrf2 positively and c-Fos and Fra1 negatively regulate the human antioxidant response element-mediated expression of NAD(P)H:quinone oxidoreductase1 gene. Proc. Natl. Acad. Sci. USA 93:14960–14965.
42. Warner, T. D., F. Giuliano, I. Vojnovic, A. Bukasa, J. A. Mitchell, and J. R. Vane. 1999. Nonsteroid drug selectivities for cyclo-oxygenase-1 rather than cyclo-oxygenase-2 are associated with human gastrointestinal toxicity: a full in vitro analysis. Proc. Natl. Acad. Sci. USA 96:7563–7568.
43. Willis, D., A. R. Moore, R. Frederick, and D. A. Willoughby. 1996. Heme oxygenase: a novel target for the modulation of the inflammatory response. Nat. Med. 2:87–90.
44. Willoughby, D. A., A. R. Moore, and P. R. Colville-Nash. 2000. Cyclopentenone prostaglandins—new allies in the war on inflammation. Nat. Med. 6:137–138.
45. Willoughby, D. A., A. R. Moore, P. R. Colville-Nash, and D. Gilroy. 2000. Resolution of inflammation. Int. J. Immunopharmacol. 22:1131–1135.
46. Yoh, K., K. Itoh, A. Enomoto, A. Hirayama, N. Yamaguchi, M. Kobayashi, N. Morito, A. Koyama, M. Yamamoto, and S. Takahashi. 2001. Nrf2-deficient female mice develop lupus-like autoimmune nephritis. Kidney Int. 60:1343–1353.

Evaluation of MafG interaction with Maf recognition element arrays by surface plasmon resonance imaging technique

Motoki Kyo[1], Tae Yamamoto[2], Hozumi Motohashi[2], Terue Kamiya[1], Toshihiro Kuroita[1], Toshiyuki Tanaka[3], James Douglas Engel[4], Bunsei Kawakami[1] and Masayuki Yamamoto[2,4,5,*]

[1]*TOYOBO Co. Ltd. Bio 21 Project, 10-24 Toyo-Cho, Tsuruga, Fukui 914-0047, Japan*
[2]*Centre for Tsukuba Advanced Research Alliance, University of Tsukuba, 1-1-1 Tennodai, Tsukuba 305-8577, Japan*
[3]*Institute of Applied Biochemistry, University of Tsukuba, 1-1-1 Tennodai, Tsukuba 305-8572, Japan*
[4]*Cell and Developmental Biology, University of Michigan Medical School, Ann Arbor, MI 48109-0616, USA*
[5]*ERATO Environmental Response Project, Japan Science and Technology Corporation, 1-1-1 Tennodai, Tsukuba 305-8577, Japan*

Specific interactions between transcription factors and *cis*-acting DNA sequence motifs are primary events for the transcriptional regulation. Many regulatory elements appear to diverge from the most optimal recognition sequences. To evaluate affinities of a transcription factor to various suboptimal sequences, we have developed a new detection method based on the surface plasmon resonance (SPR) imaging technique. Transcription factor MafG and its recognition sequence MARE (*Maf* recognition elements) were adopted to evaluate the new method. We modified DNA immobilization procedure on to the gold chip, so that a double-stranded DNA array was successfully fabricated. We further found that a hydrophilic flexible spacer composed of the poly (ethylene glycol) moiety between DNA and alkanethiol self-assembled monolayers on the surface is effective for preventing nonspecific adsorption and facilitating specific binding of MafG. Multiple interaction profiles between MafG and six of MARE-related sequences were observed by the SPR imaging technique. The kinetic values obtained by SPR imaging showed very good correlation with those obtained from electrophoretic gel mobility shift assays, although absolute values were deviated from each other. These results demonstrate that the double-stranded DNA array fabricated with the modified multistep procedure can be applied for the comprehensive analysis of the transcription factor-DNA interaction.

Introduction

Specific interactions between transcription factors and *cis*-acting DNA sequence motifs form the molecular basis of the gene expression regulation. Many preceding studies have revealed that one transcription factor usually binds to multiple related *cis*-acting motifs and, conversely, multiple related transcription factors bind to one *cis*-acting DNA motif. However, it has been very difficult technically to identify a specific and important interaction for each transcription factor and *cis*-acting motif. Detailed comparison of the binding affinities between transcription factors and specific *cis*-acting motifs therefore would provide important clue for our understanding of the transcription factor function.

The Maf family proteins appear to be typical members of a large group of regulatory factors characterized by a basic region and leucine zipper (bZip) structure (Motohashi *et al.* 2002). The founding member of this family, v-Maf, is an oncogene, which was discovered as the transforming component of the avian musculoaponeurotic fibrosarcoma virus, AS42 (Nishizawa *et al.* 1989). Subsequently, it was found that the cellular homologue, from which v-Maf was originally transduced (c-Maf), was but one member of a multigene family of related transcription factors. To date, this family consists of four large Maf family members, c-Maf, MafB, NRL, and L-Maf/A-Maf, and three small Maf proteins, MafF, MafG, and MafK (Kataoka *et al.* 1994b, 1995; Swaroop *et al.* 1992; Ogino & Yasuda 1998; Fujiwara *et al.* 1993). The proteins interacting with the small Maf family members have been expanding to include new members in Cap'n'collar (CNC) and Bach families: p45 NF-E2, Nrf1/LCR-F1, Nrf2/ECH, Nrf3, Bach1, and Bach2 (Andrews *et al.* 1993; Chan *et al.* 1993; Moi *et al.* 1994; Itoh *et al.* 1995; Kobayashi *et al.* 1999; Oyake *et al.* 1996). The superficially arbitrary division of the Maf

Communicated by: Shunsuke Ishii
**Correspondence*: E-mail: masi@tara.tsukuba.ac.jp

DOI: 10.1111/j.1365-2443.2004.00711.x

family into small and large members is likely of functional consequence, since all of the large Mafs appear to contain a recognizable transactivation domain, while the small Mafs encode slightly more than the DNA binding and dimerization motifs.

The bZip domain of the Maf factors are characterized by the presence of extended homology region (EHR), which is located in the N-terminal side of the basic region (Swaroop *et al.* 1992; ancillary DNA binding region, Kerppola & Curran 1994). DNA-binding specificity of the Maf family factors was determined by PCR-gel mobility shift assay (GMSA) amplification and purification method (Kerppola & Curran 1994; Kataoka *et al.* 1994a). Conclusion of these studies are that Maf factors recognize relatively long palindromic DNA sequences, TGCTGA$^{G}/_{C}$TCAGCA and TGCTGA$^{GC}/_{CG}$TCAGCA, which are now known as Maf recognition elements (MAREs). MAREs contain either TPA-responsive element (TRE; TGA$^{G}/_{C}$TCA) or cAMP-responsive element (CRE; TGA$^{GC}/_{CG}$TCA) as a core sequence, and extended elements on both sides of the core sequence (flanking region; 5′-TGC-core-GCA-3′). The recognition of the flanking region in MARE by EHR distinguishes the Maf family proteins from members of the AP-1 or CREB family of the bZip transcription factor superfamily. Kerppola & Curran (1994) showed evidence that the consensus sequence of large Maf binding is TGC(N)$_{6-7}$GCA. Since the flanking region of MARE is consistently required, the study strongly suggests an important contribution of the flanking region to the Maf-specific DNA-binding. Indeed, we showed that Maf EHR is important for the flanking region recognition (Kusunoki *et al.* 2002). It has also been reported through amino acid replacement/mutation analysis that a unique amino acid in the basic region is involved in the flanking region recognition by Maf proteins (Dlakic *et al.* 2001).

Currently, GMSA is a standard method to examine the interaction between transcription factors and DNA motifs and to obtain an equilibrium constant. However, GMSA is a low-throughput method for quantification of the interaction, which usually requires labourious sample preparation steps. Recently, electrodes (Boon *et al.* 2002) and surface plasmon resonance (SPR, Jost *et al.* 1991; Suzuki *et al.* 1998) techniques have been developed, and these techniques are exploited to analyse the interaction between surface immobilized molecules and those in solution. Especially, SPR has advantages that it does not require any labelled reagents and can be applied for the wide surface area (Jordan & Corn 1997). The SPR technique is especially useful for a semiquantitative analysis, as it detects a dynamic real-time interaction profile.

Another recent progress has been made in the field of chip technology, which has been applied for the study of various interactions among proteins and nucleic acid fragments as microarrays (Schena *et al.* 1995; MacBeath & Schreiber 2000; Zhu *et al.* 2001; Bulyk *et al.* 2001; Newman & Keating 2003). Indeed, Nelson *et al.* (1999) developed a prototype of imaging technique for the detection of the biomolecular interaction by combining the SPR and chip technology. This SPR imaging technique seems to enable us to analyse multiple protein–DNA interactions simultaneously and comprehensively. In this respect, SPR is more advantageous than the methods exploiting electrodes upon combination with the chip technology for a comprehensive analysis, since it would be very labourious to construct an array of tiny electrodes on a chip.

Although a multistep array fabrication procedure has been developed for the SPR-chip imaging to detect the protein-DNA interactions (Brockman *et al.* 1999), application of this technology has been hampered due to technical difficulties. In particular, double-stranded DNAs could not be directly immobilized on the chip surface, as organic solvent used in the original procedure easily denatures delicate biomolecules. In the previous procedure (Brockman *et al.* 1999), single-stranded oligonucleotides were first attached on to the gold surface followed by the hybridization with the complementary DNAs to generate double-stranded DNAs on the chip. However, in order to perform a comprehensive affinity quantification of transcription factors to various suboptimal sequences, it is required to fabricate a double-stranded DNA array composed of multiple sequences that are very similar to one another. Immobilization of preannealed double-stranded DNAs is highly preferable for preventing mismatched hybridization and for assuring complete pairing between complementary DNAs.

To develop an efficient and reliable method to detect specific protein-DNA interactions exploiting the SPR technology, we have designed in this study a modified multistep procedure for generation of DNA array on the gold surface, which does not require steps exposing DNA to noxious organic solvents. We also found a better heterobifunctional crosslinker that reduces nonspecific adsorption of the protein to the chip surface in the immobilization process. By utilizing the SPR imaging technique with the newly developed double-stranded DNA array, we then examined binding affinity of MafG, one of the small Maf family members, to several MARE-related DNA sequences. The relative affinities between MafG, various MARE-related sequences showed a very good correlation to those obtained from GMSA. Thus, the new surface immobilization procedure has enabled various delicate biomolecules, including double-stranded

DNAs, to be attached stably on to the gold chip in their native form. This procedure provides a solid basis for the study of SPR-based protein-DNA interactions.

Results

Procedure for immobilization of biomolecules on gold surface

A seven-step fabrication procedure has been used for the immobilization of biomolecules on the gold surface (Brockman *et al.* 1999), which was based on self-assembled monolayers (SAMs) of alkanethiol (Troughton *et al.* 1988; Chidsey & Loiacono 1990) and photolithography technique (Tarlov *et al.* 1993; Huang *et al.* 1994). In the procedure, the hydrophobic protecting group, 9-Fluorenylmethoxycarbonyl (Fmoc), was used for the background protection, and it was deprotected by weak base in organic solvent after single-stranded DNA was immobilized on the surface. In the final step of this procedure, an N-hydroxysuccinimido ester poly(ethylene glycol) (NHS-PEG) was reacted to an amino group on the surface. In these processes, the immobilized single-stranded DNAs were exposed to organic solvents and NHS-PEG.

In order to avoid exposure of test biomolecules to noxious effect, we established a modified procedure to fabricate double-stranded DNA array on the gold surface using thiol-terminated methoxypoly(ethylene glycol), PEG-thiol. This procedure consists of 5 steps described in Fig. 1. Step 1 is the PEG-thiol immobilization on the whole surface area of a gold slide; Step 2 is the photo-patterning by UV irradiation shielded with a bored chromium quartz mask; Step 3 is the introduction of amine terminated alkanethiol on the irradiated spots; Step 4 is the creation of maleimido surface on the spots by reacting with a heterobifunctional crosslinker, which contains a NHS ester and a maleimido group; Step 5 is the 5′-thiol-terminated DNA immobilization by thiol-maleimido coupling reaction.

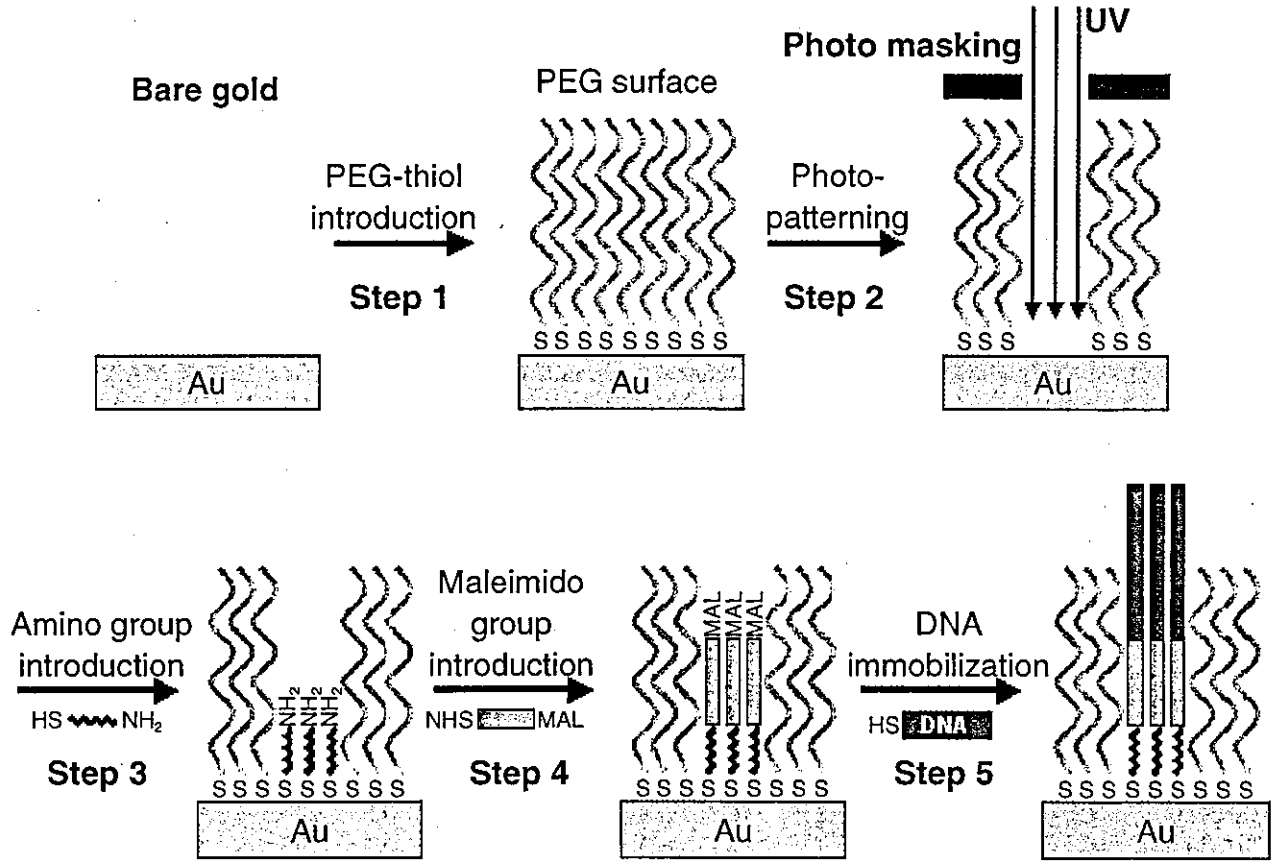

Figure 1 The scheme of surface chemistry to immobilize 5′-thiol terminated DNA. Five steps of DNA immobilization procedure are illustrated. The hydrophilic polymer, PEG-thiol, is first immobilized, which serves as the background of the array (Step 1). DNA spots are created by modifying a self-assembled monolayer of amine terminated alkanethiol, 8-AOT (Steps 2 and 3), with a heterobifunctional crosslinker to prepare a maleimido surface (Step 4). 5′-thiol terminated DNA is added to the spotted region (Step 5).

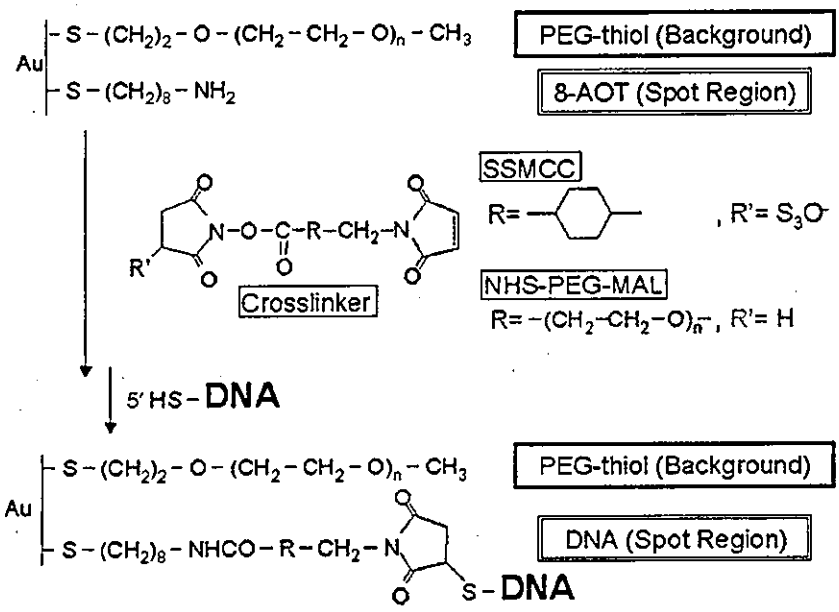

Figure 2 Two different heterobifunctional crosslinkers for specific binding of MafG to DNA array. Two heterobifunctional crosslinkers sulfosuccinimidyl-4-(*N*-maleimidomethyl)cyclohexane-1-carboxalate (SSMCC) and *N*-hydroxysuccinimide-PEG maleimido MW 3400 (NHS-PEG-MAL), were tested for the immobilization of 5′-thiol modified oligonucleotides. SSMCC provides a hydrophobic short linker, while NHS-PEG-MAL possesses a hydrophilic and flexible spacer region.

During these processes, DNA was not exposed to any organic solvents and reagents, since the DNA immobilization was the final step for the array fabrication. Therefore, this modification enabled us to fabricate an array of delicate molecules, such as double-stranded DNAs.

Heterogeneous PEG crosslinker for specific binding of MafG to DNA array

In our effort to establish a standard method for fabrication of a double-stranded DNA array, we also examined the usage of heterobifunctional crosslinkers. Two heterobifunctional crosslinkers, sulfosuccinimidyl-4-(*N*-maleimidomethyl)cyclohexane-1-carboxalate (SSMCC) and *N*-hydroxysuccinimide-PEG maleimido MW 3400 (NHS-PEG-MAL), were tested for the immobilization of 5′-thiol modified oligonucleotides (Fig. 2). SSMCC provides a hydrophobic short linker, while NHS-PEG-MAL possesses a hydrophilic and flexible spacer region.

In comparing the two above-mentioned crosslinkers, we first adopted the sequential DNA immobilization method to assure the generation of double-stranded DNAs on the surface. The reaction scheme to attach DNA on to the chip surface is shown in Fig. 2. 5′-thiol-terminated single-stranded oligonucleotides were first reacted with the maleimido moiety provided by either SSMCC or NHS-PEG-MAL, and the complementary oligonucleotides were hybridized to generate double-stranded DNAs on the surface. Two of MARE-related sequences, MARE25 and MARE23 (Kataoka *et al.* 1994a), were chosen for the assay (Table 1). MARE25 sequence completely matches the consensus sequence for the MafG homodimer binding, while MARE23 sequence has a conserved core region with the altered flanking region.

Table 1 MARE-related sequences for surface immobilization

	5′												3′
MARE25	T	G	C	T	G	A	C	T	C	A	G	C	A
hOPSIN	T	G	C	T	G	A	**T**	T	C	A	G	C	**C**
hNQO1m	**A**	G	**T**	T	G	A	C	T	C	A	G	C	A
MARE23	**C**	**A**	**A**	T	G	A	C	T	C	A	**T**	**T**	**G**
hBglHS4	**G**	G	C	T	G	A	C	T	C	A	**C**	**T**	**C**
mGSTY	T	G	**G**	T	G	A	C	**A**	**A**	A	G	C	A

The bases different from the MARE25 sequence are in bold. MARE25 contains binding motif that matches the consensus sequence for TRE-type MARE, while MARE23 sequence has a conserved core region with altered flanking region. Flanking sequence of hNQO1 MARE was modified to make the crucial G to be conserved. For this reason we named the DNA as hNQO1m.

Previous GMSA showed that MafG homodimer strongly binds to MARE25, but scarcely to MARE23, suggesting that the flanking sequence of MARE is critical for DNA binding of Maf family proteins (Kataoka *et al.* 1995).

A single-stranded DNA array with the two sequences, MARE25 and MARE23, was fabricated and sequentially exposed to 1 μM of their complementary oligonucleotides and 125 nM of MafG homodimer. Figure 3A,B show binding profiles simultaneously observed at three test spots, MARE25, MARE23 and blank (a spot with free maleimido groups), as well as one background area (a spot with free PEG-thiol groups) by SPR imaging technique. The increases of SPR signals by the addition of the complementary oligonucleotides were detected in both spots of MARE25 and MARE23, which suggests the generation of double stranded DNAs by hybridization. Importantly, no cross-hybridization was observed in these processes, indicating that the arrays were fabricated properly without base mis-pairing. When MafG was applied to the flow on the SSMCC-immobilized array, the SPR signals were increased marginally at both MARE25 and MARE23 spots, which indicates that MafG did not interact efficiently with both DNAs under this condition (Fig. 3A). On the contrary, a robust increase of SPR signal was observed for MARE25, but not for MARE23, on the NHS-PEG-MAL-immobilized array (Fig. 3B). The results were in very good agreement with the previous GMSA results, demonstrating that specific DNA-binding of MafG homodimer was reproduced on the NHS-PEG-MAL-immobilized array, but not on the SSMCC-immobilized array. Therefore, the NHS-PEG-MAL was chosen in this study for the analysis of interaction between MafG and MARE-related sequences.

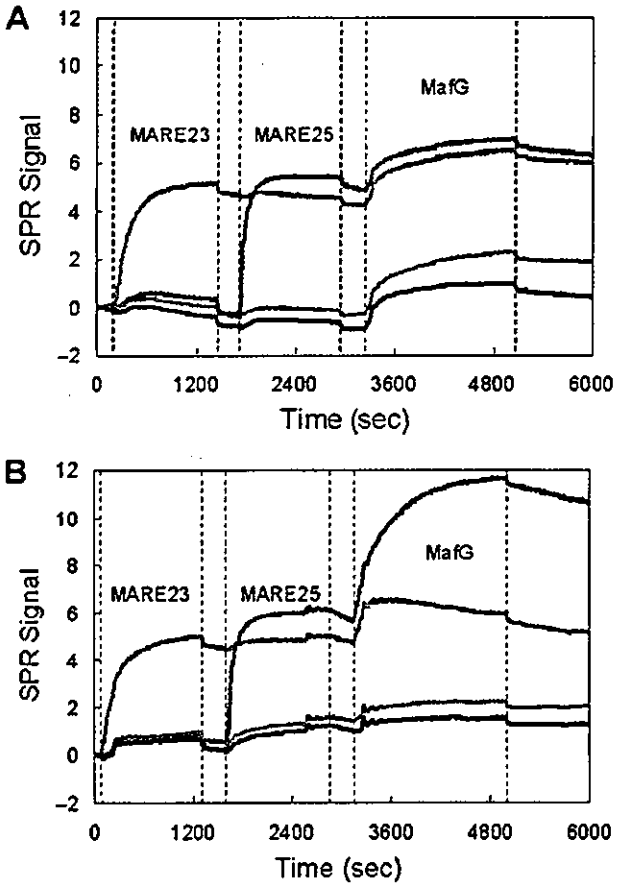

Figure 3 Sequential DNA immobilization method for generation of double-stranded DNAs on chip surface. The SPR signal changes by the exposure to 1 μM of complementary oligonucleotides of MARE25 and MARE23, and subsequently to 125 nM of MafG homodimer. The changes are monitored at MARE25 (blue), MARE23 (purple), blank (green), and background (black). Single-strand DNA was immobilized on the surface via (A) SSMCC and (B) NHS-PEG-MAL.

Salt concentration affects kinetic SPR measurements

Among various components of the SPR binding buffer, we found that the salt concentration had the greatest influence on the occurrence of nonspecific binding of transcription factors. We measured the SPR signals after continuous MafG application for 30 min at different sodium chloride concentrations from 150 mM to 300 mM (Table 2). When the sodium chloride concentration is 150 mM or less, the nonspecific binding was observed at the blank spot and PEG background on the chip, judged from the smaller value of S_1/N ratio (Table 2 and data not shown). In contrast, when 300 mM sodium chloride was applied, S_1 value (Table 2) became low, suggesting that the specific binding was inhibited. We therefore utilized intermediate concentration of sodium chloride, i.e. 200 mM, for the MafG analysis.

Under the final binding condition (20 mM HEPES-HCl (pH 7.9), 200 mM NaCl, 4 mM $MgCl_2$, 1 mM EDTA, and 100 μg/ml BSA), MafG sufficiently bound to MARE25, but not MARE23, and the kinetic data were obtained for MARE25 as k_a (association rate constant) = 4.11×10^4 (M^{-1} s^{-1}), k_d (dissociation rate constant) = 1.49×10^{-4} (s^{-1}), and K_D (dissociation constant) = 3.63×10^{-9} (M) by curve fitting calculation from simple binding model (George *et al.* 1995).

Interaction between MafG and MARE-related sequences examined on one chip

We then evaluated a double-stranded DNA array fabricated by the new immobilization method. Each pair of complementary oligonucleotides was first annealed

Table 2 Influence of salt concentration on SPR signals

NaCl concentration	SPR signal				
	MARE25 (S_1†)	MARE23 (S_2†)	Background (N†)	S_1/S_2	S_1/N
150 mM	13.40 ± 1.70	6.60 ± 0.85	5.44 ± 0.56	2.04	2.47
200 mM	20.00 ± 3.90	4.57 ± 1.83	1.24 ± 0.02	4.38	16.10
300 mM	8.07 ± 2.49	1.24 ± 0.21	1.80 ± 1.78	6.51	4.50

†SPR signals obtained after continuous MafG application for 30 min. S_1, S_2 and N are the values at the spots of MARE25, MARE23 and the background area, respectively.

and then immobilized on the surface of a gold chip. The double-stranded oligonucleotides were spotted by an automated spotter and immobilized through the thiol-modified 5′-protruding end on the gold surface via NHS-PEG-MAL. We chose four MARE-related sequences found in the regulatory regions of four endogenous genes (Table 1), including human NQO1 (hNQO1m MARE; Venugopal & Jaiswal 1996), mouse GSTy (mGSTY MARE; Itoh *et al.* 1997), human β-globin gene (hBglHS4 MARE; Stamatoyannopoulos *et al.* 1995), and human rhodopsin gene (hOPSIN MARE; Kumar *et al.* 1996). The importance of these MAREs has been examined functionally in co-transfection-transactivation analyses. The human NQO1 MARE has an altered flanking region on one side, which is similar to human β-globin MARE. To examine MAREs encompassing various categories, we modified flanking sequence of human NQO1 MARE so that the crucial 'G' in the flanking region is conserved symmetrically (Table 1). For this reason, we named the DNA as hNQO1m. In addition to these MAREs, both MARE25 and MARE23 were spotted as a positive and negative control, respectively.

The chip with the immobilized double-stranded DNAs was placed to the SPR imaging instrument, and 125 nM of MafG homodimer was applied for the DNA-protein association analysis. The SPR signal profiles of association and dissociation were observed for 1800 s with MafG-containing buffer and for the following 1200 s with the blank buffer, respectively. These results are shown in the conventional binding curves in Fig. 4A. To visualize the results more effectively, we also calculated the signals utilizing Scion Image software and the results are shown in the form of SPR difference image in Fig. 4B. The association and dissociation rate constants were calculated from the curve profiles (Fig. 4, $n = 3$) and summarized in Table 3. Although k_a and k_d values obtained from the single-stranded DNA array were slightly lower than those obtained from the double-stranded array, K_D values of MARE25 were almost the same in the two distinct

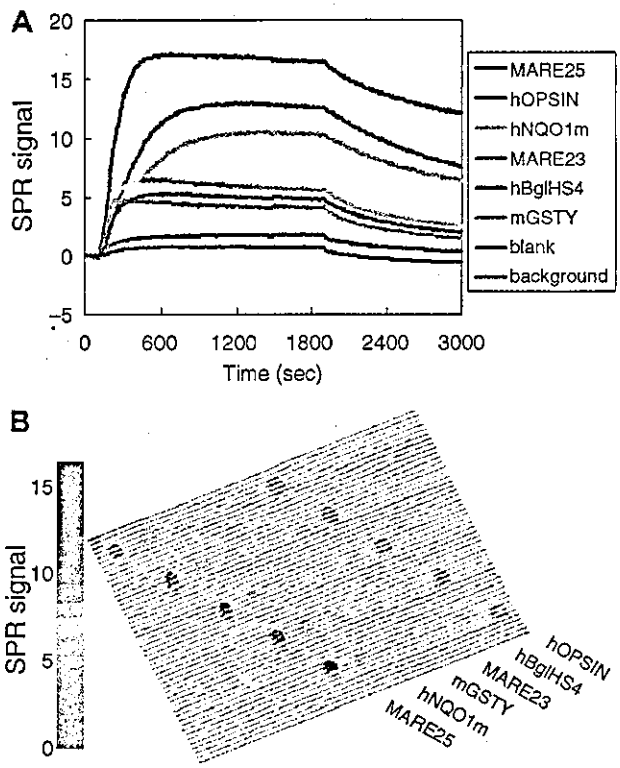

Figure 4 Interaction between MafG and MARE-related sequences examined on one chip with a double-stranded DNA array. (A) The SPR signal changes by the exposure to 125 nM MafG homodimer on the double-stranded DNA array where six MARE-like sequences are immobilized. The buffer with MafG started to flow at 0 s and was terminated at time 1800 s. The buffer without MafG was replaced and continued for the following 1200 s. Representative binding curves, each of which was obtained from a single spot, are shown. Three independent experiments were performed, and the kinetic data were calculated (see Table 3). (B) SPR difference image showing the binding of the MafG homodimer on to the double-stranded DNA array after the exposure to 125 nM MafG. Five independent spots of each oligonucleotide were generated for visualizing a representative image.

Table 3 Kinetic values of interactions between MafG homodimer and MARE-related sequences calculated from SPR profiles and GMSA

	SPR average			GMSA
	k_a [M^{-1} s^{-1}] 10^5	k_d [s^{-1}] 10^{-4}	K_D [M] 10^{-9}	K_D [M] 10^{-7}
MARE25	1.36 ± 0.32	3.13 ± 0.66	2.50 ± 1.02	2.49 ± 0.06
hOPSIN	0.50 ± 0.06	3.72 ± 0.30	7.68 ± 1.17	2.52 ± 0.05
hNQO1m	0.39 ± 0.04	3.24 ± 0.36	8.59 ± 1.75	2.73 ± 0.13
mGSTY	ND	ND	ND	ND
MARE23	ND	ND	ND	ND
hBglHS4	ND	ND	ND	ND

SPR was measured 3 times, and the average and standard deviation are shown. ND not able to determine. k_a, association rate constant; k_d, dissociation rate constant; K_D, dissociation constant.

arrays (see above and Fig. 3B). A reason for the difference in k_a and k_d values is unknown, but the similar K_D values suggest that the double-stranded DNA was properly immobilized on the surface without being denatured. The SPR difference image (Fig. 4B) was calculated from the SPR signals before and after exposure to MafG, and these signals represent that MafG properly binds to the spots. We interpret that MafG binds to MAREs specifically, since the signals on PEG background and a blank spot, where NHS-PEG-MAL is immobilized, are negligible. These results thus demonstrate successful establishment of a modified surface immobilization procedure for a double-stranded DNA array fabrication.

Kinetic data were calculated for the sequences to which substantial MafG binding was observed. Since MafG binds to DNA exclusively through forming a homodimer, it seems quite likely that observed kinetic data represent the interaction between MafG homodimer and double-stranded oligonucleotide containing MARE-related sequences. Of the six MARE and related sequences, sufficient amount of MafG interacted with MARE25, hOPSIN MARE, and hNQO1m MARE (Fig. 4). MARE25 displayed the highest affinity, and hOPSIN and hNQO1m MAREs are the next (Table 3). hOPSIN MARE has two base replacements in the MARE consensus sequence of MARE25; one is in the centre of the core region and the other is in the end of the flanking region. On the contrary, hNQO1m MARE possesses well conserved core region with mutated flanking region on one side (except that crucial G nucleotide was conserved). These observations suggest that the central bases and certain flanking bases of one side of MARE can be altered without affecting much the binding affinity to MafG. Interestingly, k_d are almost the same for MARE25, hOPSIN and hNQO1m MAREs, so the differences in K_D values should be attributable solely to those in k_a. On the other hand, MafG only weakly bound to mGSTY MARE, hBglHS4 MARE or MARE23. The results of hBglHS4 MARE and MARE23 indicate that mutations in both flanking regions eliminated the binding of MafG. Inability of mGSTY MARE to bind MafG implies that simultaneous mutations on one side of flanking region and the other side of core region may also inhibit the binding of MafG homodimer to MARE.

Comparison of K_D values obtained from SPR imaging technique and from GMSA

In order to evaluate validity of the SPR imaging technique, the K_D values obtained from the SPR binding analyses were compared to those from GMSA. The K_D values determined by GMSA for MARE25, hOPSIN MARE and hNQO1m MARE were ranged in the magnitude of 10^{-7} (Fig. 5, lanes 1–7 and 15–28). MARE25, hOPSIN MARE and hNQO1m MARE showed high affinities, and the highest was MARE25. On the contrary, weak MafG binding to mGSTY MARE was observed, albeit it was not enough for the K_D value determination (Fig. 5, lanes 29–35). No shifted bands were observed for MARE23 and hBglHS4 MARE (Fig. 5, lanes 8–14 and 36–42, respectively). These results are summarized in Table 3. Although K_D values calculated from the SPR signals are ranged in the magnitude of 10^{-9}, which are much smaller than those determined by GMSA, the comparative affinities obtained from these two distinct methods were very similar to each other. The affinity of MafG to MARE25 is the highest, and those to hOPSIN MARE and to hNQO1m MARE are intermediate. Interactions between MafG and mGSTY MARE, hBglHS4 MARE and MARE23 are not strong enough for the calculation of kinetic values.

Discussion

In this study, we have developed an improved surface chemistry suitable for the SPR-based interaction study

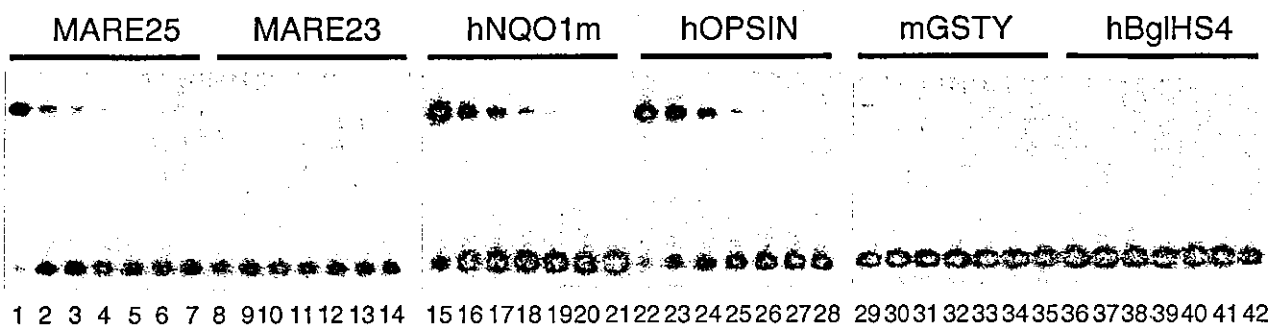

Figure 5 Interaction between MafG and MARE-related sequences observed in GMSA. Six different probes were used for GMSA, MARE25 (lanes 1–7), MARE23 (lanes 8–14), hNQO1m (lanes 15–21), hOPSIN (lanes 22–28), mGSTY (lanes 29–35) and hBglHS4 (lanes 36–42). MafG homodimer concentrations are 360 nM (lanes 1, 8, 15, 22, 29, 36), 180 nM (lanes 2, 9, 16, 23, 30, 37), 90 nM (lanes 3, 10, 17, 24, 31, 38), 45 nM (lanes 4, 11, 18, 25, 32, 39), 22.5 nM (lanes 5, 12, 19, 26, 33, 40), 11.3 nM (lanes 6, 13, 20, 27, 34, 41) and 0 nM (lanes 7, 14, 21, 28, 35, 42).

of biomolecules on the chip. In order to overcome an inconvenience that immobilized DNAs are easily denatured upon exposure to organic solvent and reactive PEG, we first constructed the background by using PEG-thiol, and test molecules were attached on to the spots in the final step. This procedure allowed pre-annealed double-stranded DNAs to be immobilized on the chip in native form. Exploiting this procedure, we successfully fabricated a double-stranded DNA array on the chip. An SPR imaging analysis based on this procedure was performed to examine the specific interaction between MafG and several MARE-related motifs. The SPR imaging analyses gave the consistent results with those obtained from GMSA as far as the relative affinities are concerned, which in turn support our contention that the detected SPR signals reflect specific binding of MafG to MAREs. Thus, this study demonstrates that the double-stranded DNA array fabricated with the modified multistep procedure can be applied for the comprehensive analysis of the transcription factor-DNA interaction.

In the classic SPR studies on the DNA-protein interaction, biotin-streptavidin chemistry was usually adopted (Seimiya & Kurosawa 1996; Galio *et al.* 1997; Suzuki *et al.* 1998; Oda *et al.* 1999). In this case, biotin-terminated oligonucleotides are usually attached on streptavidin-modified surface. This method, however, has an inherent problem upon applying for the array fabrication, as cross-contamination among the spots may happen due to a strong and quick binding reaction between biotin and streptavidin. In order to perform a comprehensive quantification of binding affinities of transcription factors to various suboptimal sequences, it is a prerequisite to fabricate a double-stranded DNA array composed of multiple sequences that are very similar to one another. To this end, we adopted a method that allows immobilization of pre-annealed double-stranded DNAs on the chip, which can prevent mismatched hybridization and attain complete pairing between complementary DNAs. Indeed, we proved in this study that correct DNA immobilization was accomplished without contaminating spots in this procedure.

Another contrivance in this procedure is the choice of NHS-PEG-MAL as a heterobifunctional crosslinker. It should be noted that the interaction profiles between MafG and MAREs obtained with NHS-PEG-MAL-immobilized array show high level consistency with those observed in GMSA. This is in stark contrast to the results with SSMCC-immobilized array, as the latter results were not consistent with the GMSA data at all. We speculate that the flexible and hydrophilic linker provided by NHS-PEG-MAL might facilitate specific binding and prevent nonspecific adsorption of MafG by allowing the higher DNA mobility. We suppose that the PEG spacer should be generally effective to avoid nonspecific interactions of a test protein to the spot background regions. On the contrary, the salt concentration required for suppression of nonspecific binding must be determined for each protein.

Interactions between transcription factors and DNAs have been investigated by several methods including GMSA (Affolter *et al.* 1990; Yamamoto *et al.* 1990), filter-binding assay (Tanikawa *et al.* 1993) and SPR (Seimiya & Kurosawa 1996; Galio *et al.* 1997; Oda *et al.* 1999). The K_D values, determined by these methods, are ranging from 10^{-7} to 10^{-10} and, especially, those obtained by SPR are from 10^{-7} to 10^{-9}. One report compared K_D values calculated by GMSA and SPR, and showed that the values are almost similar to one another ranged in the magnitude of 10^{-9} (Suzuki *et al.* 1998). In our case, K_D

values obtained by SPR ranged around 10^{-9}, while those obtained by GMSA ranged around 10^{-7} (see Table 3). While the reason for this discrepancy is unclear at present, the following two differences in the measurement conditions may be pertinent.

First, DNA mobility is different from each other in the two measurements. Whereas DNAs are immobilized on a surface for SPR analysis, they are free in the solution in GMSA. Second, optimal salt concentrations are different from each other. Buffers with higher salt concentrations (more than 150 mM) are required for the SPR measurement to avoid the nonspecific adsorption of proteins on to the chip surface or immobilized DNA. On the contrary, GMSA buffer usually contains salts less than 75 mM, and nonspecific competitor DNA is typically added to the binding reaction solutions. In fact, we utilized in this study a high salt concentration (200 mM) to suppress nonspecific binding of DNA and MafG in the SPR analysis, whereas nonspecific DNA competitor was used for this purpose in GMSA. The kinetic profiles in the SPR measurement were investigated at various salt concentrations (Seimiya & Kurosawa 1996; Oda *et al.* 1999), and it was found that the lower salt concentration gives rise to the smaller k_d values, and that k_a values are usually not affected by the salt concentration. Consistent with the finding, we found that the dissociation of MafG and MARE25 became faster when sodium chloride concentration was as high as 450 mM (data not shown). Although these results do not explain the K_D value difference between SPR and GMSA, we still consider that both SPR and GMSA measurements are valid for quantitative interaction analysis, since there is a very good correlation between the K_D values of several MAREs obtained by SPR and GMSA.

All three small Maf family proteins are known to form either homodimer or heterodimer with other bZip superfamily members, including the CNC and Bach family members, and bind to MARE (Motohashi *et al.* 2002). These partner molecules cannot bind to MARE as a monomer or homodimer, so that small Mafs confer the DNA-binding ability on partner proteins and enable them to execute various activities directed by their functional domains through the heterodimerization. Since many of these Maf-based dimers exist in cells simultaneously, it seems very difficult to identify the primary Maf molecule or to evaluate the contribution of each dimer molecule to the gene regulation through a specific MARE in the regulatory region. One simple hypothesis is to assume that the most abundant dimer molecule in the nuclei may bind dominantly to MAREs, which leads to the notion that the balance between positive and negative regulators interacting to MAREs determines the eventual transcriptional activity. In fact, by adopting megakaryocytic gene regulation directed by NF-E2 p45 and small Maf proteins, we showed that quantitative alteration enables small Maf proteins to direct both active and repressive transcription (Motohashi *et al.* 2000). In the absence of small Mafs, p45 does not bind to DNA, so MARE-dependent transcription cannot be activated. In the excess of small Mafs, transcriptionally inactive small Maf homodimer occupies MAREs and represses the transcription. Only at the optimal concentration of p45 and small Maf, the maximum level of transcriptional activation is achieved by p45/small Maf heterodimer.

Recent data suggest that the qualitative difference may also be important for the interaction of MAREs and Maf-based dimers. When we examined *mafG::mafK* compound null mutant mice, mutant animals displayed quite selective MARE-dependent transcriptional abnormality (Katsuoka *et al.* 2003). In the mice, heme oxygenase-1 (HO-1) mRNA level was markedly increased. Similarly, Bach1-null mutant mice exhibit selective increase of HO-1 mRNA level (Sun *et al.* 2002). However, no apparent influence of small Maf decrease is observed for other MARE-dependent genes (our unpublished observation), indicating that small Maf and Bach1 make a major contribution to HO-1 gene regulation.

Considering this situation, comprehensive evaluations become crucial for Maf-based dimer interactions with various MARE-related sequences. In this regard, quite recently the interactions between various bZip superfamily proteins were investigated *in silico* with glass slide-based protein arrays and fluorescent-labelled protein probes (Newman & Keating 2003). We analysed in this study the DNA-protein interaction. Our system enables to examine all possible variations in MAREs quantitatively by using a couple of gold chips or more, since simultaneous detection of 96 samples is technically feasible on one chip. We adopted MafG homodimer as our initial trial of this SPR-array technology, since it is the simple system composed of a single molecule. Obviously, next important analysis will be comparing binding profiles of MafG homodimer, Bach1/small Maf heterodimer, and the other Maf-based heterodimer molecules on one chip. We surmise that Bach1/small Maf heterodimer may have the strongest preference toward HO-1 MAREs.

In spite of discrepancy in absolute K_D values calculated from SPR and GMSA, there is a very good correlation between the two results in general. Since the SPR imaging is a powerful technique for the large-scale high-throughput analysis, we propose that the SPR imaging technique would be suitable for examining the general

binding preference of a transcription factor. We also propose that each specific interaction should be evaluated with the combination of multiple strategies, including SPR and GMSA for *in vitro* binding and reporter gene assay for *in vivo* binding.

Experimental procedures

Materials

The chemicals 8-amino-1-octanethiol, hydrochloride (8-AOT, Dojindo Laboratories), thiol terminated methoxypoly(ethylene glycol) MW 5000 (PEG-thiol, NOF), sulfosuccinimidyl-4-(*N*-maleimidomethyl)cyclohexane-1-carboxalate (SSMCC, Pierce), and *N*-hydroxysuccinimide-PEG maleimido MW 3400 (NHS-PEG-MAL, Shearwater), were all used as received.

Preparation of oligonucleotide DNAs

The oligonucleotides for covalent immobilization on the surface were designed as 5′-HS-$(T)_{15}$-CGGAAT$(N)_{13}$TTACTC-3′, and synthesized at Hokkaido System Science or Sigma Genosys with the thiol group protected. The 15-base thymine stretch with a thiol group on the 5′-end was added to the test sequence, which is composed of 13 variable sequence flanked by 6 fixed bases on both sides. 5′- and 3′-fixed sequences were CGGAAT and TTACTC, respectively. Table 1 outlines the various sequences we used in this study. The thiol group on the 5′-end of the oligonucleotides were deprotected, and they were purified by gel filtration with NAP-5 Columns (Amersham Biosciences) as described by Sigma Genosys. The complementary oligonucleotides were synthesized against the variable region with 6-base fixed regions on both sides. The double-stranded DNAs were prepared by annealing longer and shorter complementary DNAs with and without 5′-thiol group, respectively. 25 μM of 5′-thiolated strand and 100 μM of its complementary strand were annealed in the 5× SSC solution (75 mM sodium citrate, 750 mM NaCl; pH 7.0). The solution was heated to 94 °C for 5 min, and quenched to 4 °C for 15 min, then incubated at 37 °C for 3 h, to complete the annealing.

MafG protein preparation

MafG containing EHR and bZip motif, but lacking C-terminal 39 amino acids, was expressed in *Escherichia coli* as a His_6-tagged protein. The crude bacterial lysate was sequentially purified with SP sepharose (Pharmacia) and ProBond resin (Invitrogen). The recombinant protein was then cleaved with thrombin (Calbiochem) and further purified using SP sepharose. 200 μL of 125 nM MafG homodimer solution was used in one experiment.

Fabrication of DNA arrays

The covalently immobilized DNA array with PEG background was obtained by the following procedure. Gold layer (45 nm) with thin chromium underlayer (3 nm) on SF10 glass slide (Schott) were used for SPR imaging measurement. The gold slide was immersed in a PEG-thiol solution (1 mM in 1 : 6 H_2O: Ethanol) for at least 3 h to form PEG layer on the surface. This slide was patterned at 40 mW/cm^2 for 2 h with chromium quartz mask, which had 96 square holes of 500 μm, by UV light source, which was generated from a 500 W super high-pressure mercury lamp (Ushio, Tokyo). After the surface was rinsed with water and ethanol, the slide was soaked in 1 mM ethanolic solution of 8-AOT for 1 h. This resulted in 96 amino-functionalized 500 μm squares with PEG background. Thiol-reactive maleimido-modified surface was created with 1 mM solution of heterobifunctional crosslinker SSMCC or NHS-PEG-MAL in phosphate buffer (20 mM phosphate; pH 7.0 and 100 mM NaCl). 10 nL drop of 10 μM 5′-thiol-terminated DNA in phosphate buffer was delivered automatically on the patterned surface by using an automated spotter (Toyobo, Osaka), and the reaction was carried out for overnight. Then the surface was rinsed with phosphate buffer and 5× SSC solution containing 0.1% SDS.

SPR imaging analysis

The DNA array was placed immediately in the SPR imaging instrument (Toyobo). The SPR signals were obtained in the SPR buffer (20 mM HEPES (pH 7.9), 200 mM NaCl, 4 mM $MgCl_2$, 1 mM EDTA, and 100 μg/mL BSA). The SPR buffer and the sample in the same buffer were applied to the array surface with 100 μl/min. The SPR image and signal data were collected with MultiSPRinter Analysis program (Toyobo). The SPR difference image was constructed by using Scion Image (Scion, MD USA). The kinetic values were calculated with the program based on the simple reversible reaction model (George *et al.* 1995).

Gel mobility shift assays

Gel mobility shift assays were performed as previously described (Kataoka *et al.* 1994a). The same oligonucleotides with those used in SPR detection, which are composed of a 13 bp-variable sequence flanked by 6 bp-fixed regions on both sides, were end labelled with γ-^{32}P-ATP for generating probes. MafG protein was incubated with probes in the gel shift buffer (20 mM HEPES (pH 7.9), 20 mM KCl, 5 mM dithiothreitol, 4 mM $MgCl_2$, 1 mM EDTA, 100 μg/mL BSA and 400 μg/mL poly(dIdC)) at 37 °C for 30 min. The resulting mixture was subjected to native polyacrylamide gel electrophoresis and visualized by autoradiography. The K_D values were determined as described (Azam & Ishihama 1999) on the basis of the results obtained using protein concentration from 0 to 360 μM.

Acknowledgements

We are grateful to Ms Kit Tong for critical reading of the manuscript. This work was supported by grants from ERATO (MY), the Ministry of Education, Culture, Sports, Science, and Technology (H.M. and M.Y.), the Ministry of Health, Labor and Welfare (M.Y.), CREST (H.M.), PROBRAIN (H.M.), and Special Coordination Fund for Promoting Science and Technology (H.M.).

References

Affolter, M., Percival-Smith, A., Muller, M., Leupin, W. & Gehring, W.J. (1990) DNA binding properties of the purified Antennapedia homeodomain. *Proc. Natl. Acad. Sci. USA* **87**, 4093–4097.

Andrews, N.C., Erdjument-Bromage, H., Davidson, M.B., Tempst, P. & Orkin, S.H. (1993) Erythroid transcription factor NF-E2 is a haematopoietic-specific basic-leucine zipper protein. *Nature* **362**, 722–728.

Azam, T.A. & Ishihama, A. (1999) Twelve species of the nucleoid-associated protein from *Escherichia coli*. Sequence recognition specificity and DNA binding affinity. *J. Biol. Chem.* **274**, 33105–33113.

Boon, E.M., Salas, J.E. & Barton, J.K. (2002) An electrical probe of protein–DNA interactions on DNA-modified surfaces. *Nature Biotechn.* **20**, 282–286.

Brockman, J.M., Fruto, A.G. & Corn, R.M. (1999) A multi-step chemical modification procedure to create DNA arrays on gold surfaces for the study of protein–DNA interaction with surface plasmon resonance imaging. *J. Am. Chem. Soc.* **121**, 8044–8051.

Bulyk, M.L., Huang, X., Choo, Y. & Church, G.M. (2001) Exploring the DNA binding specificities of zinc fingers with DNA microarrays. *Proc. Natl. Acad. Sci. USA* **98**, 7158–7163.

Chan, J.Y., Han, X. & Kan, Y.W. (1993) Cloning of Nrf1, an NF-E2-related transcription factor, by genetic selection in yeast. *Proc. Natl. Acad. Sci. USA* **90**, 11371–11375.

Chidsey, C.E.D. & Loiacono, D.N. (1990) Chemical functionality in self-assembled monolayers: structural and electrochemical properties. *Langmuir* **6**, 682–691.

Dlakic, M., Grinberg, A.V., Leonard, D.A. & Kerppola, T.K. (2001) DNA sequence-dependent folding determines the divergence in binding specificities between Maf and other bZIP proteins. *EMBO J.* **20**, 828–840.

Fujiwara, K.T., Kataoka, K. & Nishizawa, M. (1993) Two new members of the *maf* oncogene family, *maf*K and *maf*F, encode nuclear b-Zip proteins lacking putative trans-activator domain. *Oncogene* **8**, 2371–2381.

Galio, L., Briquet, S., Cot, S., Guillet, J.G. & Vaquero, C. (1997) Analysis of interactions between huGATA-3 transcription factor and three GATA regulatory elements of HIV-1 long terminal repeat, by surface plasmon resonance. *Anal. Biochem.* **253**, 70–77.

George, A.J., French, R.R. & Glennie, M.J. (1995) Measurement of kinetic binding constants of a panel of anti-saporin antibodies using a resonant mirror biosensor. *J. Immunol. Methods* **183**, 51–63.

Huang, J., Dahlgren, D.A. & Hemminger, J.C. (1994) Photopatterning of self-assembled alkanethiolate monolayers on gold: a simple monolayer photoresist utilizing aqueous chemistry. *Langmuir* **10**, 626–628.

Itoh, K., Chiba, T., Takahashi, S., *et al.* (1997) An Nrf2/small Maf heterodimer mediates the induction of phase II detoxifying enzyme genes through antioxidant response elements. *Biochem. Biophys. Res. Commun.* **236**, 313–322.

Itoh, K., Igarashi, K., Hayashi, N., Nishizawa, M. & Yamamoto, M. (1995) Cloning and characterization of a novel erythroid cell-derived CNC family transcription factor heterodimerizing with the small Maf family proteins. *Mol. Cell. Biol.* **15**, 4184–4193.

Jordan, C.E. & Corn, R.M. (1997) Surface plasmon resonance imaging measurements of electrostatic biopolymer adsorption onto chemically modified gold surfaces. *Anal. Chem.* **69**, 1449–1456.

Jost, J.P., Munch, O. & Andersson, T. (1991) Study of protein–DNA interactions by surface plasmon resonance (real time kinetics). *Nucl. Acids Res.* **19**, 2788.

Kataoka, K., Fujiwara, K.T., Noda, M. & Nishizawa, M. (1994a) MafB, a new Maf family transcription activator that can associate with Maf and Fos but not with Jun. *Mol. Cell. Biol.* **14**, 7581–7591.

Kataoka, K., Igarashi, K., Itoh, K., *et al.* (1995) Small Maf proteins heterodimerize with Fos and potentially act as competitive repressors of NF-E2 transcription factor. *Mol. Cell. Biol.* **15**, 2180–2190.

Kataoka, K., Noda, M. & Nishizawa, M. (1994b) Maf nuclear oncoprotein recognizes sequences related to an AP-1 site and forms heterodimers with both Fos and Jun. *Mol. Cell. Biol.* **14**, 700–712.

Katsuoka, F., Motohashi, H., Tamagawa, Y., *et al.* (2003) Small Maf compound mutants display central nervous system neuronal degeneration, aberrant transcription, and Bach protein mislocalization coincident with myoclonus and abnormal startle response. *Mol. Cell. Biol.* **23**, 1163–1174.

Kerppola, T.K. & Curran, T.A. (1994) A conserved region adjacent to the basic domain is required for recognition of an extended DNA binding site by Maf/Nrl family proteins. *Oncogene* **9**, 3149–3158.

Kobayashi, A., Ito, E., Toki, T., *et al.* (1999) Molecular cloning and functional characterization of a new Cap'n'collar family transcription factor Nrf3. *J. Biol. Chem.* **274**, 6443–6452.

Kumar, R., Chen, S., Scheurer, D., *et al.* (1996) The bZIP transcription factor Nrl stimulates rhodopsin promoter activity in primary retinal cell cultures. *J. Biol. Chem.* **271**, 29612–29618.

Kusunoki, H., Motohashi, H., Katsuoka, F., Morohashi, A., Yamamoto, M. & Tanaka, T. (2002) Solution structure of the DNA-binding domain of MafG. *Nature Struct. Biol.* **9**, 252–256.

MacBeath, G. & Schreiber, S.L. (2000) Printing proteins as microarrays for high-throughput function determination. *Science* **289**, 1760–1763.

Moi, P., Chan, K., Asunis, I., Cao, A. & Kan, Y.W. (1994) Isolation of NF-E2-related factor 2 (Nrf2), a NF-E2-like basic leucine zipper transcriptional activator that binds to the tandem NF-E2/AP1 repeat of the beta-globin locus control region. *Proc. Natl. Acad. Sci. USA* **91**, 9926–9930.

Motohashi, H., Katsuoka, F., Shavit, J.A., Engel, J.D. & Yamamoto, M. (2000) Positive or negative MARE-dependent transcriptional regulation is determined by the abundance of small Maf proteins. *Cell* **103**, 865–875.

Motohashi, H., O'Connor, T., Katsuoka, F., Engel, J.D. & Yamamoto, M. (2002) Integration and diversity of the

regulatory network composed of Maf and CNC families of transcription factors. *Gene* **294**, 1–12.

Nelson, B.P., Frutos, A.G., Brockman, J.M. & Corn, R.M. (1999) Near-infrared surface plasmon resonance measurements of ultrathin films. 1. Angle shift and SPR imaging experiments. *Anal. Chem.* **71**, 3928–3934.

Newman, J.R. & Keating, A.E. (2003) Comprehensive identification of human bZIP interactions with coiled-coil arrays. *Science* **300**, 2097–2101.

Nishizawa, M., Kataoka, K., Goto, N., Fujiwara, K.T. & Kawai, S. (1989) v-maf, a viral oncogene that encodes a 'leucine zipper' motif. *Proc. Natl. Acad. Sci. USA* **86**, 7711–7715.

Oda, M., Furukawa, K., Sarai, A. & Nakamura, H. (1999) Kinetic analysis of DNA binding by the c-Myb DNA-binding domain using surface plasmon resonance. *FEBS Lett.* **454**, 288–292.

Ogino, H. & Yasuda, K. (1998) Induction of lens differentiation by activation of a bZIP transcription factor, L-Maf. *Science* **280**, 115–118.

Oyake, T., Itoh, K., Motohashi, H., *et al.* (1996) Bach proteins belong to a novel family of BTB-basic leucine zipper transcription factors that interact with MafK and regulate transcription through the NF-E2 site. *Mol. Cell. Biol.* **16**, 6083–6095.

Schena, M., Shalon, D., Davis, R.W. & Brown, P.O. (1995) Quantitative monitoring of gene expression patterns with a cDNA microarray. *Science* **270**, 467–470.

Seimiya, M. & Kurosawa, Y. (1996) Kinetics of binding of Antp homeodomain to DNA analyzed by measurements of surface plasmon resonance. *FEBS Lett.* **398**, 279–284.

Stamatoyannopoulos, J.A., Goodwin, A., Joyce, T. & Lowrey, C.H. (1995) NF-E2 and GATA binding motifs are required for the formation of DNase I hypersensitive site 4 of the human beta-globin locus control region. *EMBO J.* **14**, 106–116.

Sun, J., Hoshino, H., Takaku, K., *et al.* (2002) Hemoprotein Bach1 regulates enhancer availability of heme oxygenase-1 gene. *EMBO J.* **21**, 5216–5224.

Suzuki, F., Goto, M., Sawa, C., *et al.* (1998) Functional interaction of transcription factor human GA-binding protein subunits. *J. Biol. Chem.* **273**, 29302–29308.

Swaroop, A., Xu, J., Pawer, H., Jackson, A., Scolnick, C. & Agarwal, N. (1992) A conserved retina-specific gene encodes a basic motif/leucine zipper protein. *Proc. Natl. Acad. Sci. USA* **89**, 266–270.

Tanikawa, J., Yasukawa, T., Enari, M., *et al.* (1993) Recognition of specific DNA sequences by the c-myb protooncogene product: role of three repeat units in the DNA-binding domain. *Proc. Natl. Acad. Sci. USA* **90**, 9320–9324.

Tarlov, M.J., Burgess, D.R.F. & Gillen, J.G. (1993) UV photopatterning of alkanethiolate monolayers self-assembled on gold and silver. *J. Am. Chem. Soc.* **115**, 5305–5306.

Troughton, E.B., Bain, C.D., Whitesides, G.M., Nuzzo, R.G., Allara, D.L. & Porter, M.D. (1988) Monolayer films prepared by the spontaneous self-assembly of symmetrical and unsymmetrical dialkyl sulfides from solution onto gold substrates: structure, properties, and reactivity of constituent functional groups. *Langmuir* **4**, 365–385.

Venugopal, R. & Jaiswal, A.K. (1996) Nrf1 and Nrf2 positively and c-Fos and Fra1 negatively regulate the human antioxidant response element-mediated expression of NAD (P) H: quinone oxidoreductase1 gene. *Proc. Natl. Acad. Sci. USA* **93**, 14960–14965.

Yamamoto, M., Ko, L.J., Leonard, M.W., Beug, H., Orkin, S.H. & Engel, J.D. (1990) Activity and tissue-specific expression of the transcription factor NF-E1 [GATA] multigene family. *Genes Dev.* **4**, 1650–1662.

Zhu, H., Bilgin, M., Bangham, R., *et al.* (2001) Global analysis of protein activities using proteome chips. *Science* **293**, 2101–2105.

Received: 17 October 2003
Accepted: 26 November 2003

Role of Nrf2 in the Regulation of CD36 and Stress Protein Expression in Murine Macrophages

Activation by Oxidatively Modified LDL and 4-Hydroxynonenal

Tetsuro Ishii, Ken Itoh, Emilio Ruiz, David S. Leake, Hiroyuki Unoki, Masayuki Yamamoto, Giovanni E. Mann

Abstract—CD36 is an important scavenger receptor mediating uptake of oxidized low-density lipoproteins (oxLDLs) and plays a key role in foam cell formation and the pathogenesis of atherosclerosis. We report the first evidence that the transcription factor Nrf2 is expressed in vascular smooth muscle cells, and demonstrate that oxLDLs cause nuclear accumulation of Nrf2 in murine macrophages, resulting in the activation of genes encoding CD36 and the stress proteins A170, heme oxygenase-1 (HO-1), and peroxiredoxin I (Prx I). 4-Hydroxy-2-nonenal (HNE), derived from lipid peroxidation, was one of the most effective activators of Nrf2. Using Nrf2-deficient macrophages, we established that Nrf2 partially regulates CD36 expression in response to oxLDLs, HNE, or the electrophilic agent diethylmaleate. In murine aortic smooth muscle cells, expressing negligible levels of CD36, both moderately and highly oxidized LDL caused only limited Nrf2 translocation and negligible increases in A170, HO-1, and Prx I expression. However, treatment of smooth muscle cells with HNE significantly enhanced nuclear accumulation of Nrf2 and increased A170, HO-1, and Prx I protein levels. Because PPAR-γ can be activated by oxLDLs and controls expression of CD36 in macrophages, our results implicate Nrf2 as a second important transcription factor involved in the induction of the scavenger receptor CD36 and antioxidant stress genes in atherosclerosis. (*Circ Res.* 2004;94:609-616.)

Key Words: CD36 ■ Nrf2 ■ oxidized LDL ■ macrophages ■ vascular smooth muscle cells

Low-density lipoprotein (LDL) is susceptible to oxidative damage, and oxidatively modified LDL (oxLDL) plays a key role in the development of atherosclerotic lesions.[1,2] OxLDL is taken up via different scavenger receptors, and in macrophages, CD36, SR-A, and LOX-1 are the predominant receptors.[3–5] Enhanced formation of oxLDL in the vascular wall induces the formation of foam cells that accumulate cholesterol.[1–4] LDL oxidation is associated with the formation of a number of highly reactive molecules, such as lipid peroxides, lysophosphatidylcholine, oxysterols, and aldehydes,[6] which cause vascular inflammation and fibrosis[7,8] and expression of antiinflammatory genes in macrophages[9] and vascular smooth muscle cells.[10]

Components of oxLDL, such as 9-HODE and 13-HODE, activate peroxisome proliferator-activated receptor γ (PPAR-γ), resulting in the upregulation of the major oxLDL receptor CD36.[11] PPAR-γ appears to inhibit inflammatory response genes by antagonizing the activities of AP-1, NF-κB, and Stat 1 transcription factors.[12,13] Moreover, macrophages derived from mice in which the PPARγ gene has been "floxed out" fail to upregulate CD36 expression in response to treatment with thiazolidinedione drugs such as rosiglitazone.[14,15]

Our previous studies in vivo established that the transcription factor Nrf2, which interacts with electrophile (EpRE) and antioxidant (ARE) response elements and regulates expression of the detoxifying enzymes GST and NQO1 in tissues in response to dietary 2(3)-*t*-butyl-4-hydroxyanisole.[16] Moreover, the sensitivity to carcinogenesis is increased in Nrf2-deficient mice due to the loss of induction of ARE-regulated drug metabolizing enzymes and antioxidant genes,[17,18] and Nrf2 has also been implicated in the protection against oxidative damage induced by hyperoxia.[19] Thus, Nrf2 serves as a key transcription factor in the cytoprotection of tissues against electrophiles and reactive oxygen species.

We previously reported that Nrf2 regulates expression of HO-1, Prx I, anionic amino acid transporter xCT, and the ubiquitin/PKC-ζ–interacting protein A170 in murine peritoneal macrophages.[20] Activation of Nrf2 by electrophilic agents or reactive oxygen species is controlled by a

Original received March 19, 2003; resubmission received December 16, 2003; revised resubmission received January 14, 2004; accepted January 16, 2004.

From the Institutes of Community Medicine (T.I.) and Basic Medical Sciences (K.I., H.U., M.Y.), University of Tsukuba, Tsukuba, Japan; Cell and Molecular Biology Research Division (D.S.L.), School of Animal and Microbial Sciences, University of Reading, UK; Centre for Cardiovascular Biology and Medicine (E.R., G.E.M.), GKT School of Biomedical Sciences, King's College London, Guy's Campus, London, UK.

Correspondence to Prof Tetsuro Ishii, Institute of Community Medicine, University of Tsukuba, Tsukuba 305-8575, Japan. E-mail teishii@md.tsukuba.ac.jp and Prof Giovanni E. Mann, Centre for Cardiovascular Biology and Medicine, GKT School of Biomedical Sciences, King's College London, Guy's Campus, London SE1 1UL, UK. E-mail giovanni.mann@kcl.ac.uk

Circulation Research is available at http://www.circresaha.org DOI: 10.1161/01.RES.0000119171.44657.45

novel cytoplasmic protein designated Keap 1 that interacts with Nrf2 and negatively regulates nuclear translocation of Nrf2 and facilitates degradation of Nrf2 via the proteasome.[21,22]

OxLDLs upregulate HO-1 and Prx I expression in murine macrophages[11] and porcine aortic smooth muscle cells,[23] whereas immunostaining and in situ hybridization have established that HO-1 is prominently expressed in the endothelium and foam cells/macrophages in the intima of atherosclerotic lesions in humans and mice.[24] HO-1 plays an essential antiinflammatory role in vitro and in vivo,[25] and Prx I due its thioredoxin peroxidase activity can reduce hydrogen peroxide[26] and modulate H_2O_2-mediated activation of NF-κB.[27]

We have investigated the role of Nrf2 in the induction of stress proteins by oxLDLs and 4-hydroxynonenal (HNE) in murine peritoneal macrophages and aortic smooth muscle cells (SMCs) isolated from wild-type and *nrf2*-knockout mice. We show for the first time that oxLDLs activate Nrf2 in murine macrophages, but less efficiently in SMCs, and that HNE, one of the major end products of lipid oxidation and contained in oxLDL, is a potent activator of Nrf2 translocation to the nucleus in both cell types. Moreover, we provide novel evidence that Nrf2 is an important regulator of CD36 expression in murine macrophages. Because PPAR-γ can be activated by oxLDLs and controls expression of CD36 in macrophages, our results implicate Nrf2 as an additional transcription factor involved in the regulation oxLDL uptake by the vascular wall and induction of antioxidant stress genes in atherosclerosis.

Materials and Methods

Reagents

4-Hydroxy-2-nonenal (HNE) and 15-deoxy-$\Delta^{12,14}$-PGJ_2 (15d-PGJ_2) were from Calbiochem, rosiglitazone was from Cayman Chemical, HPODE was from Biomol, monoclonal antibody reactive with murine CD36 was from Cascade Biosciences, and Dr Western (marker for Western blot) was from Oriental Yeast Co. Ltd. All other chemicals, actin antibody (A-2066), lysophosphatidylcholine (LPC), 7-ketocholesterol, hexanal, malondialdehyde, and 7β-hydroxycholesterol were from Sigma Chemical Co.

Culture of Mouse Peritoneal Macrophages and Aortic Smooth Muscle Cells

Mouse peritoneal macrophages were prepared from female ICR mice and *nrf2*-knockout mice backcrossed with ICR mice that 4 days previously received an intraperitoneal injection of 2 mL of 4% thioglycollate broth.[20] Additional experiments were performed using peritoneal macrophages from *CD36*-deficient female mice. Macrophages were maintained in RPMI 1640 medium (10% fetal calf serum), chemical agents added and cultured as indicated. Explant cultures of mouse aortic smooth muscle cells (SMCs) were maintained in Dulbecco's modified Eagle's medium (10% fetal calf serum), and experiments conducted with passage 5 to 10 cells. Animal experimental procedures were in accordance with University of Tsukuba's Regulations on Animal Experiments and Japanese Governmental Law No. 105.

Preparation of LDL

LDL was isolated from normal human blood by ultracentrifugation in the presence of EDTA as described previously.[10] Oxidatively modified LDLs were formed by incubating LDL with 5 μmol/L $CuSO_4$ at 37°C, and the conjugated diene content determined by measuring absorbance at 234 nm. Lipid hydroperoxides in native (nLDL), moderately oxidized LDL (moxLDL), and highly oxidized LDL (oxLDL) were 40, 64, and 80 nmol/mg protein, respectively, and the relative electrophoretic mobilities of moxLDL and oxLDL (compared with native LDL) were 1.3 and 4.6, respectively.

Western Blot Analysis

Before electrophoresis, a marker dye and 2-mercaptoethanol were added to lysates, which were then fractionated by SDS-polyacrylamide gel electrophoresis and electrotransferred onto an Immobilon membrane (Millipore).[20] Polyclonal rabbit antisera raised against purified rat HO-1, rat Prx I, and recombinant mouse A170 and Nrf2 were used. Nuclear pellets were prepared after cell lysis in 0.5% Nonidet P-40 containing buffer.[20] Densitometric analysis was performed using NIH Image software.

Northern Blot Analysis

Total RNA was extracted from cells using RNeasy (QIAGEN), fractionated by electrophoresis and transferred to Zeta-Probe GT membranes (Bio-Rad). Membranes were probed with [^{32}P]-labeled cDNA prepared by Megaprime labeling (Amersham), using 18S rRNA cDNA as an internal control. As described previously,[21] cDNA fragments for A170, HO-1, Prx I, and CD36 were prepared from Bluescript plasmid and used for hybridization.

Reverse Transcription–PCR Analysis

Oligonucleotide primers used for RT-PCR were as follows: 5′-TGTGCTAGACATTGGCAAATG-3′ and 5′-CTTCTCCTAAAGATAGGTGTG-3′ for detecting mouse CD36 mRNA, 5′-AAAGATAGACACCATCACCC-3′ and 5′-GCGACAGTCAAAAGTCTTCTC-3′ for mouse LOX-1 mRNA, 5′-TCTCTACCTCCTTGTGTTTG-3′ and 5′-GATTGCATCCAGTGAATTCC-3′ for mouse macrophage scavenger receptor I (SR-A) mRNA, and 5′-TGAAGGTCGGAGTCAACGGATTTGGT-3′ and 5′-CATGTGGGCCATGAGGTCCACCAC-3′ for mouse GAPDH mRNA. Total RNAs isolated from macrophages treated with moxLDL or oxLDL for 24 hours were analyzed by RT-PCR using a QIAGEN OneStep RT-PCR kit. An aliquot of each RT-PCR mixture was electrophoresed on a 1.2% agarose gel and stained with Vistra Green (Amersham Pharmacia Biotech). The signal intensity of the RT-PCR products was determined using Fluoroimager 595 (Amersham Pharmacia Biotech). The amounts of total RNA templates and cycle numbers for amplification were chosen in quantitative ranges determined by plotting signal intensities as functions of the template amounts and cycle numbers. Nucleotide sequences of the RT-PCR products were verified.

Oil Red O Staining

Mouse peritoneal macrophages were incubated for 24 hours at 37°C in 5% CO_2 in RPMI 1640 medium containing 10% FCS in the absence or presence of HNE (10 μmol/L) or moxLDL or oxLDL (200 μg protein mL^{-1}). Macrophages were washed twice, fixed in formalin, and stained with oil red O. The area of lipid-loaded macrophages was measured using a computerized MacSCOPE image analysis system (Mitani Corp).

Results

Oxidatively Modified LDL Activates Nrf2 in Peritoneal Macrophages

The effects of oxLDLs on nuclear accumulation of Nrf2 and stress gene expression in murine macrophages are shown in Figure 1. Cells were pretreated for 5 hours with nLDL, moxLDL, and oxLDL, and nuclear fractions were analyzed by immunostaining. Nuclear levels of Nrf2 were enhanced markedly after treatment with either moxLDL or oxLDL, whereas nLDL increased Nrf2 translocation marginally (Fig-

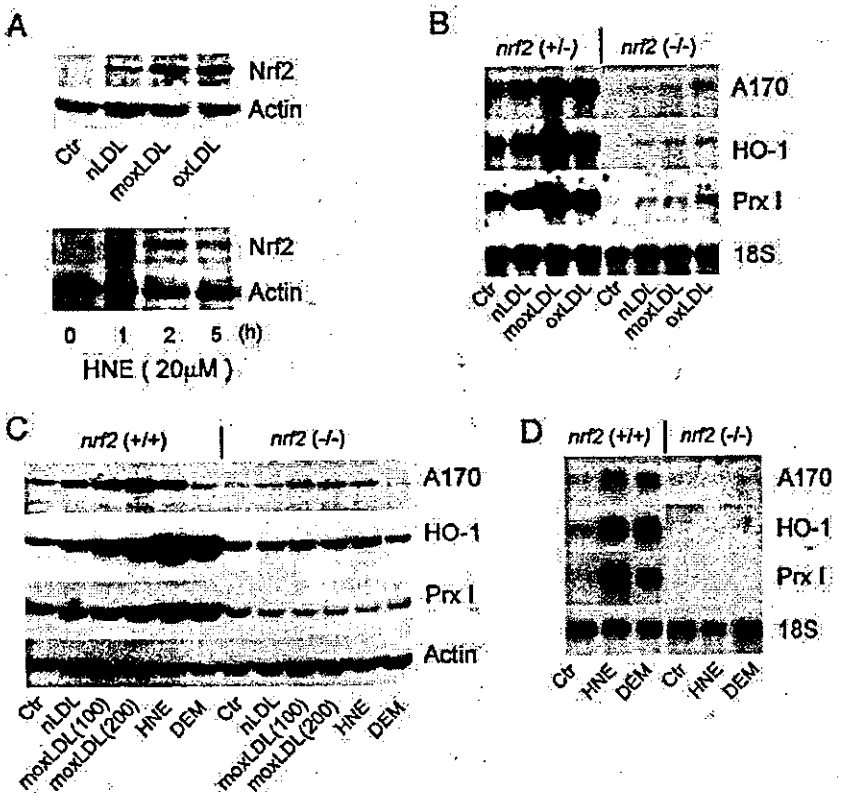

Figure 1. OxLDL and HNE induced nuclear accumulation of Nrf2 and A170, HO-1, and Prx I expression in peritoneal macrophages. A, Nrf2 and actin (internal control) in nuclear fractions were detected by immunoblot analysis. Top, Cells were incubated for 5 hours in the absence (Ctr) or presence of 100 μg protein mL^{-1} native LDL (nLDL), moderately oxidized LDL (moxLDL), or highly oxidized LDL (oxLDL). Bottom, Time-dependent nuclear accumulation of Nrf2 in cells treated with 20 μmol/L HNE. Nuclear fractions were prepared from control (0 hours) and HNE-treated (1 to 5 hours) wild-type cells. B, Nrf2-dependent upregulation of A170, HO-1, and Prx I mRNA (5 hours) by 250 μg protein mL^{-1} nLDL, moxLDL, and oxLDL in $nrf2^{+/-}$ and $nrf2^{-/-}$ cells. Ribosomal 18S RNA was used as an internal control. C, A170, HO-1, Prx I, and actin (internal control) protein expression in $nrf2^{+/+}$ and $nrf2^{-/-}$ macrophages incubated for 8 hours in the absence (Ctr) or presence of nLDL (100 μg protein mL^{-1}) or moxLDL (100 or 200 μg protein mL^{-1}), HNE (20 μmol/L), or diethylmaleate (100 μmol/L). D, Nrf2-dependent upregulation of A170, HO-1, and Prx I mRNA levels in cells treated for 5 hours with either 20 μmol/L HNE or 100 μmol/L DEM.

ure 1A, top). Increased Nrf2 levels induced by these agents were also detected in whole cell lysates (data not shown).

When effects of oxLDLs (5 hours) on A170, HO-1, and Prx I mRNA levels were determined in heterozygous mutant and Nrf2-deficient (homozygous mutant) macrophages, both moxLDL and oxLDL increased A170, HO-1, and Prx I mRNA levels (relative to 18S rRNA) in $nrf2^{+/-}$ cells, whereas nLDL had a negligible effect (Figure 1B). Basal expression of these transcripts was significantly lower in $nrf2^{-/-}$ compared $nrf2^{+/-}$ (or wild type, data not shown) macrophages, and oxLDLs caused only marginal increases in mRNA levels (Figure 1B). moxLDL only caused a concentration-dependent increase in A170, HO-1, and Prx I expression in $nrf2^{+/+}$ macrophages. In $nrf2^{-/-}$ cells, moxLDL only slightly enhanced A170 levels but did not increase expression of either HO-1 or Prx I (Figure 1C).

Effects of LDL Components on Induction of Stress Proteins

Because oxidized LDL contains lipid hydroperoxides, oxysterols, and aldehydes,[1,6,28] we examined the effects of lysophosphatidylcholine (LPC), HPODE, 7-ketocholesterol, hexanal, malondialdehyde, 7β-hydroxycholesterol, and 4-hydroxy-2-nonenal (HNE). Treatment of macrophages for 8 hours with either LPC (50 μmol/L), 7-ketocholesterol (20 and 40 μmol/L), or hexanal (250 and 500 μmol/L) had no significant effect on A170, HO-1, and Prx I expression, whereas HPODE or malondialdehyde only slightly enhanced protein levels at 50 μmol/L (data not shown). 7β-Hydroxycholesterol increased A170, HO-1, and Prx I expression only at concentrations above 50 μmol/L (data not shown). We found that HNE was the most effective activator of Nrf2-mediated increases in stress protein mRNA and protein levels (Figures 1C and 1D). The estimated content of HNE in highly oxidized LDL is 114 nmol/mg LDL protein,[6] corresponding to ≈17 μmol/L HNE when 150 μg protein mL^{-1} oxidized LDLs were added to culture media. These results suggest that HNE contained in oxidized LDL could be one of the activators of Nrf2.

4-Hydroxynonenal Activates Nrf2 and Stress Protein Expression in Peritoneal Macrophages

HNE increased nuclear translocation of Nrf2 after 1 to 5 hours (Figure 1A, bottom). HNE and diethylmaleate (DEM), a typical Nrf2-activating electrophilic agent,[20] increased stress protein expression in $nrf2^{+/+}$ macrophages, with responses markedly attenuated in $nrf2^{-/-}$ cells (Figures 1C and 1D).

Effects of Oxidatively Modified LDL and HNE in Murine Aortic Smooth Muscle Cells

In contrast to our findings in macrophages, oxLDLs had a negligible effect on nuclear translocation and accumulation of Nrf2 in murine aortic smooth muscle cells (SMCs) (Figure 2A, top). In contrast, a rapid (1 to 3 hours), transient increase in nuclear Nrf2 levels was observed in SMCs treated with HNE (Figure 2A, bottom). When the effects of oxLDLs, HNE, and DEM on transcriptional activation of A170, HO-1, and Prx I were examined in $nrf2^{+/+}$ SMCs under standard culture conditions, relatively

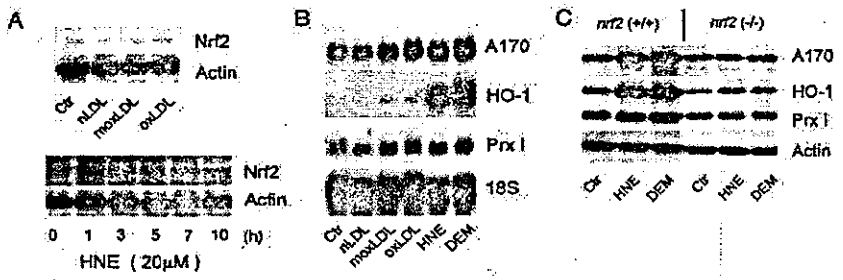

Figure 2. Activation of Nrf2 and enhanced expression of A170, HO-1, and Prx I in murine aortic smooth muscle cells. A, Nrf2 and actin (internal control) in nuclear fractions were detected by immunoblot analysis. Top, Cells were treated for 5 hours in the absence (Ctr) or presence of 100 μg protein mL^{-1} nLDL, moxLDL, oxLDL. Bottom, Time-dependent nuclear accumulation of Nrf2 in SMCs treated with 20 μmol/L HNE. Nuclear fractions were prepared from *nrf2*$^{+/+}$control (0 hours) and HNE-treated (1 to 10 hours) SMCs. B, A170, HO-1, and Prx I mRNA levels in SMCs treated for 5 hours with 100 μg protein mL^{-1} nLDL, moxLDL, and oxLDL, 20 μmol/L HNE, or 100 μmol/L DEM. C, Immunoblot showing A170, HO-1, and Prx I expression in *nrf2*$^{+/+}$ and *nrf2*$^{-/-}$ SMCs treated for 8 hours with 20 μmol/L HNE or 100 μmol/L DEM.

high basal mRNA levels were detected for Prx I and A170, whereas basal HO-1 mRNA levels were low (Figure 2B). Notably, nLDL, moxLDL, and oxLDL failed to increase mRNA (Figure 2B) or protein (data not shown) levels for A170, HO-1, and Prx I in *nrf2*$^{+/+}$ SMCs.

HNE and DEM significantly increased mRNA and protein levels of A170 and HO-1 in *nrf2*$^{+/+}$ SMCs, whereas Prx I expression was only slightly enhanced (Figures 2B and 2C). In *nrf2*$^{-/-}$ SMCs, neither HNE nor DEM affected A170, HO-1, and Prx I expression (Figure 2C). Thus, as in macrophages, increased stress protein expression in SMCs induced by HNE or DEM is largely dependent on activation of Nrf2, establishing a strong correlation between nuclear accumulation of Nrf2 and transcriptional activation of stress genes.

Activation of CD36 Gene Expression by HNE and DEM in Murine Peritoneal Macrophages

CD36 is the major scavenger receptor for the uptake of oxidatively modified LDL in macrophages.[3–5,29,30] We previously isolated the mouse homologue of a CD36 cDNA clone,[31] and in the present study, Northern blot analysis showed that HNE and DEM increased CD36 mRNA levels in *nrf2*$^{+/+}$ but not *nrf2*$^{-/-}$ macrophages (Figure 3A, top). Immunoblot experiments established that HNE and DEM (8 hours) caused a 2.2-fold and 1.4-fold increase in CD36 protein levels in *nrf2*$^{+/+}$ macrophages, whereas upregulation of CD36 was minimal in *nrf2*$^{-/-}$ cells (Figure 3A, bottom). These findings suggest that increased CD36 expression in response to HNE and DEM is largely dependent on the activation of Nrf2. As basal expression of CD36 in *nrf2*$^{+/+}$ and *nrf2*$^{-/-}$ macrophages was similar (Figure 3A, bottom), this suggests that Nrf2 does not modulate basal CD36 expression.

Nrf2-Dependent Upregulation of CD36 Expression by Oxidatively Modified LDL

We could not detect upregulation of CD36 protein levels in macrophages treated with moxLDL or oxLDL for 8 hours (Figure 3A, bottom), and therefore examined concentration-

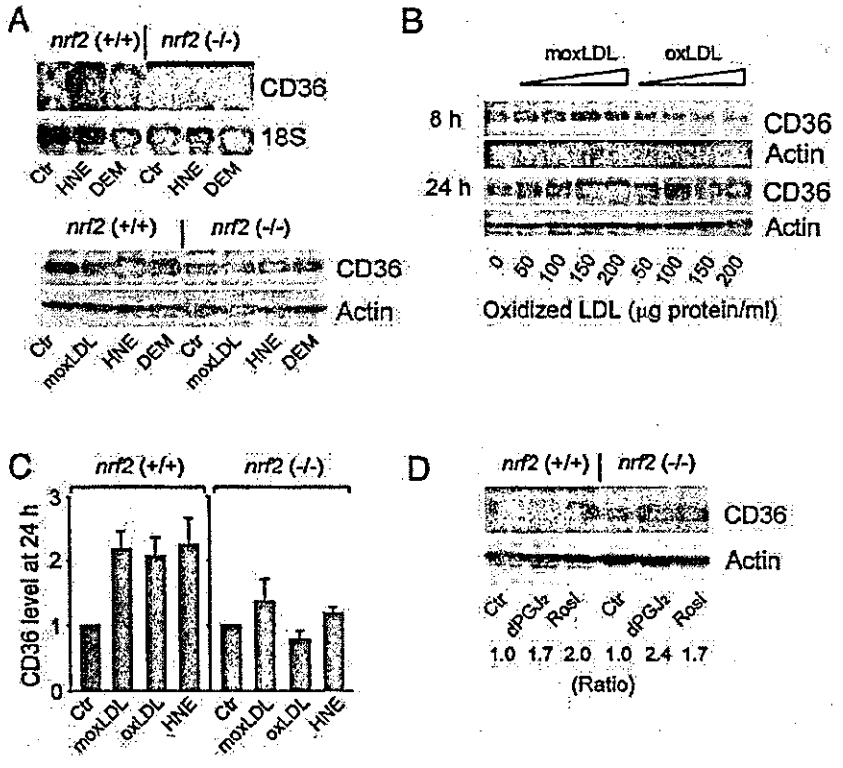

Figure 3. Nrf2-dependent induction of CD36 expression in murine peritoneal macrophages. A, Top, CD36 mRNA levels in *nrf2*$^{+/+}$ and *nrf2*$^{-/-}$ macrophages treated for 5 hours with 20 μmol/L HNE or 100 μmol/L DEM. Bottom, Immunoblot comparing CD36 protein levels in *nrf2*$^{+/+}$ and *nrf2*$^{-/-}$ macrophages treated for 8 hours with 100 μg protein mL^{-1} moxLDL, 20 μmol/L HNE, or 100 μmol/L DEM. B, Immunoblot showing CD36 expression in *nrf2*$^{+/+}$ macrophages treated either for 8 or 24 hours in the absence (Ctr) or presence of 50 to 200 μg protein mL^{-1} moxLDL or oxLDL. C, Densitometric analysis of 24-hour treatment with moxLDL, oxLDL, or HNE (20 μmol/L) on CD36 expression in *nrf2*$^{+/+}$ and *nrf2*$^{-/-}$ macrophages. Values denote mean±SEM of experiments in 3 to 5 different cell cultures. D, Effects of PPARγ activators on CD36 protein levels in *nrf2*$^{+/+}$ and *nrf2*$^{-/-}$ macrophages. Cells were treated for 24 hours in the absence (Ctr) or presence of 5 μmol/L 15d-prostaglandin J_2 (dPGJ$_2$) or 5 μmol/L rosiglitazone (Rosi).

dependent effects of moxLDL and oxLDL (50 to 200 μg protein mL^{-1}) on CD36 expression at 8 and 24 hours in *nrf2*$^{+/+}$ macrophages. moxLDL and oxLDL dose-dependently increased CD36 levels only after 24 hours (Figure 3B). When effects of moxLDL and oxLDL (200 μg protein mL^{-1}, 24 hours) were compared in *nrf2*$^{+/+}$ and *nrf2*$^{-/-}$ macrophages, induction of CD36 was significantly attenuated in Nrf2-deficient macrophages (Figure 3C). HNE markedly increased CD36 levels in *nrf2*$^{+/+}$ macrophages but was less effective in *nrf2*$^{-/-}$ macrophages, providing the first direct evidence that Nrf2 is important in the activation of CD36 gene expression in macrophages exposed to oxLDLs or HNE.

Similar experiments with SMCs failed to detect CD36 mRNA and protein expression under basal conditions or after treatment with 100 μg protein mL^{-1} nLDL, moxLDL or oxLDL, HNE (20 μmol/L, 5 to 8 hours), or DEM (100 μmol/L, 5 to 8 hours) (data not shown).

PPAR-γ Activators Upregulate CD36 Expression in Nrf2-Deficient Macrophages

PPAR-γ plays an important role in the induction of CD36 by oxLDLs.[11,32,33] Under our experimental conditions, CD36 expression was upregulated in *nrf2*$^{+/+}$ and *nrf2*$^{-/-}$ macrophages by the PPAR-γ activators 15d-PGJ_2 and rosiglitazone (Figure 3D), indicating that PPAR-γ activation of CD36 gene expression occurs via a signaling pathway distinct from Nrf2.

Effects of Oxidatively Modified LDL on Expression of Other Scavenger Receptors

We used quantitative RT-PCR to compare CD36, LOX-1, and SR-A mRNA levels in murine macrophages. In contrast to upregulation of CD36 in response to moxLDL and oxLDL (Figure 4A), mRNA levels for LOX-1 were downregulated whereas levels for SR-A remained unchanged (data not shown). Our findings are consistent with a previous report that increased uptake of oxLDL in monocytes is the result of increased expression of CD36 but not of the scavenger receptor SR-A type I or type II.[34] Oil red O staining of macrophages revealed that moxLDL significantly enhanced the accumulation of cholesterol in *nrf2*$^{+/+}$ cells, whereas the intensity of staining was much lower in Nrf2-deficient cells (see Figures 4B and 4C). HNE alone only slightly enhanced oil red O staining in both cell types. These results indicate that Nrf2-dependent upregulation of CD36 leads to an accumulation of cholesterol in macrophages treated with moderately oxidized LDL. However, experiments with *CD36*$^{-/-}$ peritoneal macrophages revealed that CD36 is not essential for activation of Nrf2 by oxLDL or HNE (data not shown).

Discussion

We report the first evidence that oxLDLs and HNE induce nuclear translocation of Nrf2 in murine peritoneal macrophages, resulting in an upregulation of the scavenger receptor CD36 and antioxidant stress proteins A170, HO-1, and Prx I. Our study establishes (1) Nrf2 as a novel signaling pathway involved in the regulation of CD36 gene expression in macrophages, (2) HNE as a potent activator of Nrf2 in both macrophages and SMCs, and (3) oxLDLs as effective activators of Nrf2 in macrophages but not in SMCs expressing negligible levels of CD36. In addition to identifying Nrf2 as a key transcription factor controlling antioxidant gene expression, our findings implicate Nrf2 as an important signaling pathway in atherosclerosis.

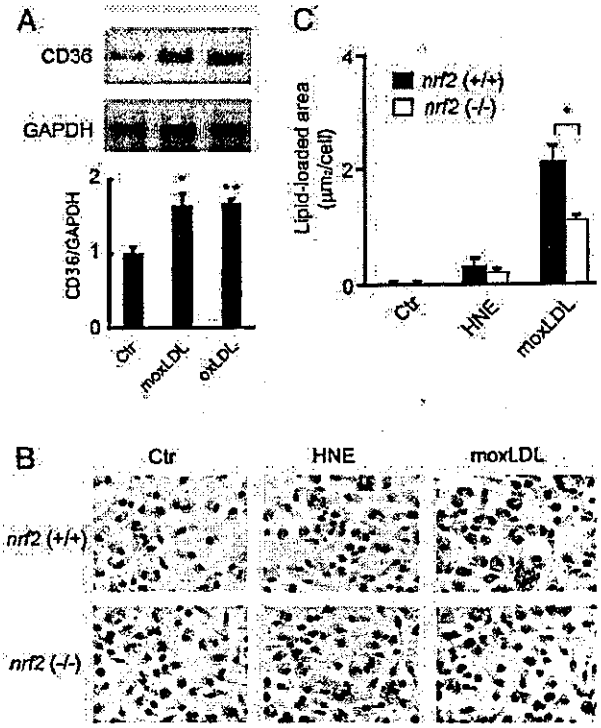

Figure 4. Effects of oxLDLs and HNE on CD36 expression and cholesterol accumulation in peritoneal macrophages. A, RT-PCR analysis of CD36 gene expression in cells treated for 24 hours in the absence (Ctr) or presence of 200 μg protein mL^{-1} moxLDL or oxLDL, using GAPDH mRNA as a loading control. B, Oil red O staining of *nrf2*$^{+/+}$ and *nrf2*$^{-/-}$ macrophages treated for 24 hours in the absence (Ctr) or presence of 10 μmol/L HNE or 200 μg protein mL^{-1} moxLDL. C, Lipid-loaded area of ~150 to 200 macrophages measured by oil red O staining. Values denote mean±SEM of measurements in 3 different experiments. $^{*}P<0.05$, $^{**}P<0.01$.

In macrophages, CD36 can be upregulated by oxLDL,[29,30] and previous studies have established an integral role for PPAR-γ in CD36 gene expression.[11,32] PPAR-γ modulates lipid homeostasis and antiinflammatory responses in macrophages[33] and is expressed at high levels in foam cells in atherosclerotic lesions.[11,35] PPAR-γ–deficient macrophages express low levels of both CD36 mRNA and protein, suggesting that PPAR-γ controls basal levels of CD36.[15] However, the latter study did not examine whether oxLDLs enhance CD36 expression in PPAR-γ–deficient macrophages. We have identified Nrf2 as a novel signaling pathway, distinct from PPAR-γ, that also upregulates CD36 expression in macrophages treated with oxLDLs. The following evidence supports this conclusion. First, HNE readily enters cells and is highly reactive with proteins and metabolized by enzymes such as aldo-keto-reductase.[28] Second, HNE does not activate